NUST COLLEGE OF ELECTRICAL & MECHANICAL ENGINEERING

Development of Liquid Piston Stirling Engine

Final Year Project (FYP) Report

Department of Mechanical Engineering, EME, NUST

Group Members

Adeel Ahmed

M. Kashif Khan

Hassan Zamir Khan

M. Hassaan Yousaf

Supervisor

Asst. Prof. Dr. Abdur Rehman Mazhar

June 10th, 2022

ACKNOWLEDGEMENT

All power resides with Almighty Allah for He bestowed us with the utmost guidance and strength to see through this venture. We are grateful to the heartfelt prayers and support of our friends and family that thoroughly kept our morale high. The pursuit of knowledge is impossible without a worthy mentor and thereby we are obliged to have the wisdom of our supervisor Dr Raja Amir Azim who expertly guided us through every step of our way. We will always be grateful to his persistent confidence in our work that made us achieve our aspirations and can never forget the key contributions of our faculty as well that laid the very basis of our engineering journey

DECLARATION

We hereby declare that no portion of the work referred to in this Project Thesis has been submitted in support of an application for another degree or qualification of this of any other university or other institute of learning. If any act of plagiarism found, we are fully responsible for every disciplinary action taken against us depending upon the seriousness of the proven offence, even the cancellation of our degree

COPYRIGHT STATEMENT

Table of Contents

LIST OF FIGURES

LIST OF TABLES

Abstract

Stirling engines are a type of reciprocating external combustion engines that use one or more pistons to achieve useful work through some input of heat from an external source. The liquid piston heat engine, also known as the Fluidyne design, utilizes liquid water as pistons that are enclosed in a cylinder which entraps a working gas. Stirling engines are low efficiency engines that can utilize waste and low-grade thermal energy to pump water at a small scale. Exploiting these low-grade waste and renewable energies provides significant opportunities for addressing the energy related problems, such as energy safety and shortage, greenhouse gas emission, water dissipation, etc. Due to the great capability of recovering low-grade heat with potentially high efficiencies, Stirling cycle engines have attracted increasing attention in recent decades. Due to their low power density and efficiency use of fluidyne pumps at a small scale may be very useful. Liquid pistons avoid the sliding mechanical seal and accurately dimensioned cylinders, which provide great flexibility mechanical design with much simpler constructions. With the implementation of fluidyne pumps both the requirements efficient utilization of energy sources and a shift to renewable resources are fulfilled. This research will raise awareness for the neglected way of using renewable source to pump water especially the use of biomass. The research will also cover that what effects are observed when in a fluidyne engine the water levels are changed and the effect of using a mixture of different working liquids of low heats of vaporization.

***Keywords*: Stirling engine, Pumping, Sustainability, Low-Grade Heat, Fluidyne Engine, External Combustion Engine.**

1 Introduction

Sustainable pumping techniques are of great value in countries depending heavily on their agricultural output with farms scattered over distant areas and remote regions with electricity unavailability. Laying down electrical transmission lines to these scarcely populated areas with low power requirements is not an economical argument. Even if accessibility to fuel to power generators is made possible skilled maintenance of such machinery is not an easy task. In this scenario, use of sustainable resources of energy is a very economical proposition that cannot go noticed and is an area of interest.

With use of sustainable and renewable energy methods the waste energy or heat which is an omni-present part of life can also not go unnoticed. Even in the most developed countries such as the US 60% of heat is unrecovered reason being the expenses associated in the infrastructure for recovering that waste energy. Capture of low-quality heat with temperatures less than 150 °C is an effort demanding task which is limited by the efficiencies of the systems utilized for this purpose. This is mainly due to the Carnot limit where the efficiency is limited by the hot and cold sink temperatures as shown below.

$$\eta_{carnot} = 1 - \frac{T_{Cold}}{T_{Hot}} \qquad \mathbf{1}$$

A solution to this is to approach the capture of the waste energy while focusing on reducing the expenses of a heat recovering system. An efficiency limited system can have useful applications given that operational costs of the system are less than the useful work obtained given the fact that waste heat is abundant and mostly unutilized.

A liquid piston heat engine offers unparalleled potential to both renewable and waste-heat recovering methods regarding its low manufacturing and operational costs. The engine is composed simply of a working fluid and a working gas retained in a certain geometry by

inexpensive and easily manufactured materials. Because the working fluid can be water and the working gas air, the low cost of construction and available materials offers a great deal of potential in certain niche applications. These engines by their nature are inclined towards pumping applications and could become an important segment of active heat transfer and water management techniques in regions where maintenance and resources are limited as mentioned earlier.

Other than its direct value addition to the present world, liquid piston Stirling cycle engines indirectly add value through the knowledge and research perspective. Their simple designs let to simple data collection and quantitative analysis offering simpler demonstration of thermodynamics for learning purposes of students.

In this type of engine liquid columns act as pistons, when the height of the liquid columns oscillates the working gas is transferred between hot and cold regions. As the liquid columns act as pistons these engines provide ease in not having to manufacture accurate pistons and cylinders and sliding mechanical seals. These engines are also possible in several designs in which the liquid in columns can be separated by air from the water to be pumped or be liquid coupled. These designs are simpler than those of the other types of the Stirling engines. With the simple designs the fluidyne engines come with easy assembling too requiring few plastic tubes, a few 2- or 3-point connectors, a metal conductive pipe and a pair of non-returning valves. The materials required in the assembly of fluidyne engine demonstration are of usual daily use and can be found easily in household items making them very cheap relatively to the other types of Stirling engines.

1.1 Definitions

For the better understanding of the fluidyne engines it is preferrable to familiarize with some terms.

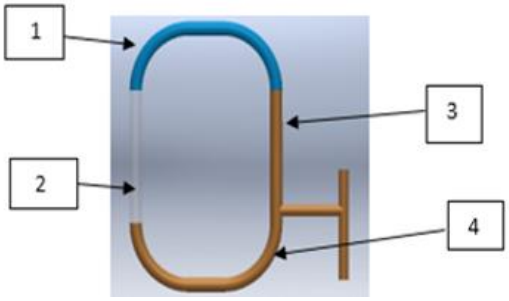

Figure 1. Schematic of the engine.

1) Gas chamber: Gas-phase portion of the engine containing the working gas and vapor.
2) Cold column: Liquid containing column not exposed to heating source.
3) Hot column: Liquid containing column exposed to heating source.
4) Displacer: Liquid chamber of engine connecting hot and cold columns.

Other than these terms a few more terms should also be known (not depicted in above figure).

5) Working liquid: The liquid-phase working fluid which composes the liquid columns and displacer.
6) Working vapor: Vaporized form of working liquid.
7) Working gas: non-condensable gas contained in gas chamber which in our case was air all the time.
8) Heater: As a source of heat, a hot air gun was utilized of variable power outputs.

Figure 2. Hot air gun used as a heating source.

1.2 Working Principle

For the complete understanding of the liquid piston Stirling cycle engines, it is important to know and understand the basic operation of Stirling engine. The basic principle of the Stirling engine is a simple one: it relies only on the fact that when a gas is heated, it tends to expand or, if confined, to a rise in pressure.

Stirling engines work by the repeated heating and cooling of a sealed amount of working gas which in our case will be air. The gas follows the behavior described by the gas laws which describe how a gas' pressure, temperature and volume are related. When the gas is heated, because it is in a sealed chamber, the pressure rises, and this then acts on the power piston to produce a power stroke. When the gas is cooled, the pressure drops and this means that less work needs to be done by the piston to recompress the gas on the return stroke, giving a net gain in power available on the shaft. The working gas flows cyclically between the hot and cold heat exchangers.

The Stirling cycle is represented in the P-v and T-s diagrams as shown below:

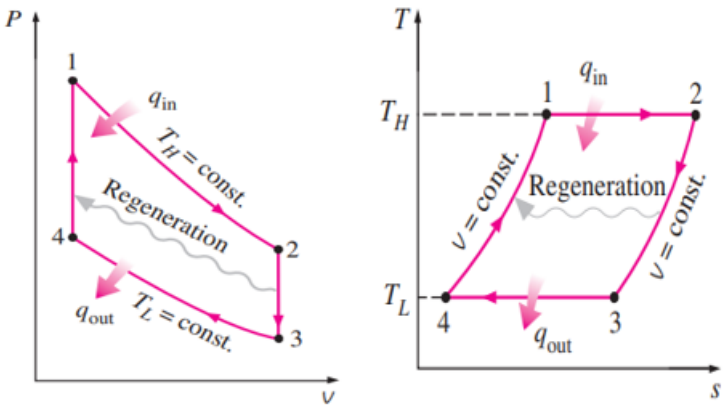

Figure 3. P-V and T-s diagrams of Stirling engines (reprinted from Y. A. Cengel & M.A. Boles [1]).

<u>1 – 2: Isothermal Expansion</u>

The working gas (air in our case) expands as heat Q_{in} is transferred to the expansion space of the engine. The gas expands and does work (usually work is done on a power piston), causing

the engine volume to increase and the pressure to decrease. Assuming isothermal conditions ($T=T_H$), the heat transferred to the working gas is exactly $Q_h=W_e$, where W_e is the work done on the power piston.

2 – 3: Isochoric Displacement (Cooling)

The working gas is moved through the regenerator at the maximum engine volume. Heat is transferred from the working gas to the regenerator, causing the pressure, temperature and entropy of the gas to decrease.

3 – 4: Isothermal Compression

The cooled working gas is compressed (usually by a power piston) in the compression space, and heat Q_C is sunk to the cold reservoir at constant temperature T_L. Consequently, the engine volume decreases, while the engine pressure increases. Assuming isothermal conditions ($T=T_L$), the heat sunk to the surroundings is exactly $Q_C=W_C$, where W_C is the work done by the power piston on the working gas.

4 – 1: Isochoric Displacement (Heating)

The working gas is moved through the regenerator at the minimum engine volume. Heat is transferred from the regenerator to the working gas, causing the pressure, temperature and entropy of the gas to increase.

1.3 Perturbations

In the liquid piston engines under focus here, the working fluid is vaporized at the hot end and condensed at the cold end. This creates a circular mass flow of vapor and liquid along the length of gas chamber between the liquid columns. It is to note that only the mass flow and heat transfer does not cause the volumetric oscillations necessary for pumping and the perturbation caused by the vaporization of liquid in hot column is also required for the pumping. The

vaporization or the boiling forms a small but erratic pressure differential that jeopardizes the U formation of liquid in displacer and the columns into unstable position. To equalize this imbalance, liquid oscillation occurs back in hot column but overshoots the initial equilibrium exposing more liquid in hot column and causing more vaporization. With the correct calibration, the initial perturbation creates a positive feedback loop in which the working liquid begins oscillating back and forth between the hot and cold columns at a characteristic frequency and amplitude. This oscillation of liquid leads in a variation of flow of vapor mass and volume between hot and cold ends. The combined effect of this and oscillating liquid shuttles the working gas between hot and cold ends and the gas is made to work in a Stirling cycle. The following diagram explain the processes further.

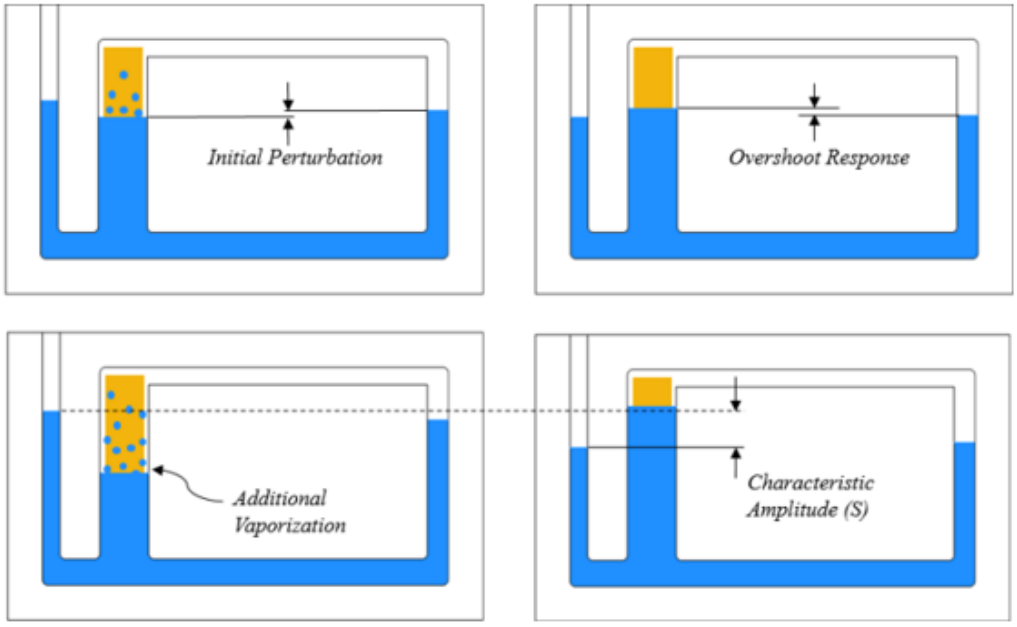

Figure 4. Engine oscillation beginning with Initial Perturbation then Equilibrium overshoot then Periodic liquid in cold column to Periodic liquid in hot column (reprinted from S.Newlan [2], Copyright Shawn Newlan 2017).

2 Literature Review

Liquid piston Stirling engines, also known as ‘‘fluidyne’’ engines, use liquid pistons rather than the solid pistons found in conventional engines. This eliminates the need for manufacturing high tolerance parts and constant maintenance of the engine. They are low in cost and are easy to construct. Due to the engine’s low thermal efficiency, it is limited to certain applications. [3].

The working principles and dynamics of Fluidyne engines have been theoretically explained by works of many researchers. Early work on Fluidyne engines divided them in two concepts. Based on these concepts they are either classified as liquid coupled or gas coupled. These are shown in figure below.

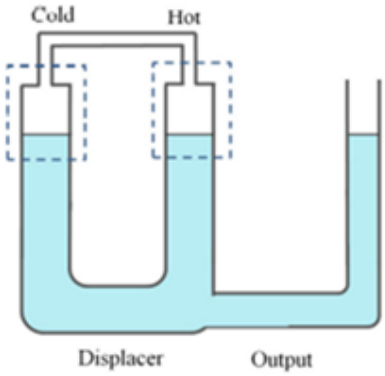

Figure 5. Basic Configuration of a fluidyne engine (reprinted from K. Wang et al. [4], Copyright 2016 from Elsevier).

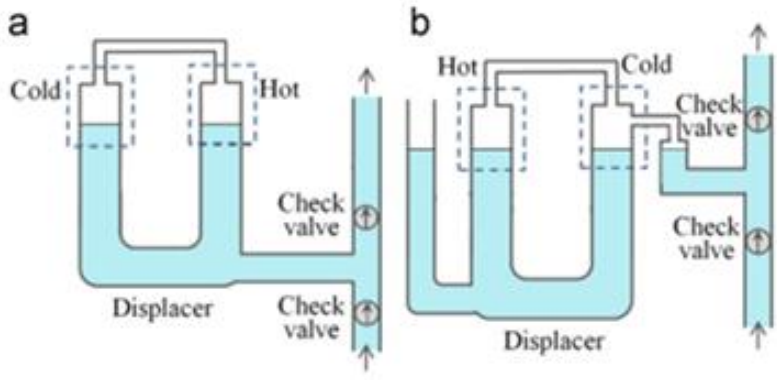

Figure 6. (a) Liquid coupled and (b) Gas coupled (reprinted from K. Wang et al. [4], Copyright 2016 from Elsevier).

Comparing these two types reveal that the liquid coupled offers high power density, operable on lower temperature differential and has simpler, smaller design in contrast to large, complex design of gas coupled, with low power density but higher temperature differential and efficiency.

The first experimental fluidyne engine was produced by Colin West in 1971. This engine possesses operability at pressures close to atmospheric, temperatures less than 100°C and low frequency, typically around 1 Hz. Dr. West and his group at Oak Ridge National Labs (ORNL) were pioneers in the research, collaboration, and distribution of information regarding liquid piston engines with primary application for large scale water pumps and wrote the book: *The Liquid Piston Stirling Engine* giving a basic and generalized review along with design choices and future implications of these engines [5].

Based on the Fluidyne engine designed by West, more similar prototypes were later built and tested at University of the Witwatersrand in 1976 and more findings were shared at 12th intersociety energy conversion engineering conference in 1977 [6,7]. In 1979, more work on the behavior of fluidyne engines operating at lower temperature of below 350 K was shared by C.W Stammers. In this work dry air closed regenerative cycle was assumed and an expression was derived to approximate the value of temperature difference required to attain small oscillations in pump. Viscous losses and velocity dependent load were admitted and scenario of pumping against a head was also considered [8].

The following Stirling engine was built and tested by Yang et al. [9]. He integrated a two-cylinder Fluidyne engine, as shown in the figure below. The design achieved spontaneous oscillation at a constant 2.2 W heating power per cylinder with a maximum peak amplitude of 10.5 mm in the output column at 7 W per cylinder. The tested operating frequency was around 2.53 Hz. The pumping operation of the Fluidyne engine showed that the two-cylinder engine

reached flow rates of 23 ml/min for a zero head, and 19 ml/ min for a head of 5 cm. The efficiency of the engine was 0.1% when provided with 4 W of heat per cylinder, and 0.016% when operated for pumping.

Empirical study of different water pumps by gathering their efficiency and pumping capacity data was carried out by Orda and Mahkamov [10]. In their study the analyzed three prototypes, one using a heated element in concentric cylinder, another which employed flat-plate solar collector in a U-tube design and last using a compact form improvised the second design. Their study though based on experimental data from their own models laid out physical data of solar heated fluidyne engines which can operate under varying conditions of solar collection and pumping requirements. Similarly, Jackson W. Mason and colleagues also utilized a testbed of Fresnel Lens as heating source by focusing Sunlight on the hot side of the fluidyne [11,12]. For simulation of a real-world scenario movement of the Sun was compensated for the test run. They used instruments like thermocouples, differential pressure transducer, a liquid level measurement device and a data acquisition system for data retrieving. They found out that unlike typical IC engines which are physically constrained to operate with the same displacement but can vary their speed, the fluidyne engine operates with constant ‘‘speed’’ but can vary the displacement. The result of larger liquid piston movements is higher friction. The performance is shown by the Beale number, a parameter that characterizes the performance of Stirling engines. The dynamic mechanical response showed no delay from the thermodynamic expansion due to temperature changes of the working fluid. The constant speed nature of the fluidyne engine means that increases in heat input result in greater piston displacement for an unloaded engine.

A solar powered fluidyne pump for irrigational pumping was built and tested by Bell [13]. Two displacer cylinders were connected to either side of a water-filled U-tube. To extract work a diaphragm pump was used. The diaphragm pump made use of an area difference to amplify

the pressure attained in the water to be pumped and hence the pump head of the device. Laboratory tests on a small scale fluidyne heat engine in loaded and unloaded configurations were conducted by Mosby [14]. These tests evaluated the effect of geometric changes on system's operating characteristics. Liquid column displacements, gas temperatures and pressure were the primarily measured variables for various heat inputs and volumes of gas.

Presently the efficiencies of fluidyne engines achieved lies in range from 5-10 %. This has limited the use of these engines to applications with energy available at no cost mainly solar and waste. Literature review gathered has revealed numerous model designs operating in dry mode and wet mode with varying efficiencies, but these models are limited by the relevant assumptions and resources of the researchers. It is also seen that insufficient understanding of principles of fluidyne operation and lack of focus from researchers has inhibited the growth in research in this field and efficiencies of these engines as well. In fact, this type of Stirling cycle engines are the least researched and practically tested engines. With so many areas of this field unexplored it represent a good opportunity for new researchers in this field. For this, a hand sized model of fluidyne engine is designed, constructed and utilized for research in this paper for developing and validating more accurate analytical description and trends of the fluidyne process.

3 Methodology

In pursuit of our project objectives, we start with implementing gathered literature review to come up with a working hand model of a fluidyne engine in unloaded or basic configuration. Pumping mechanism comprising of two non-returning valves will then be integrated to the hand model. Improvements, regular maintenance of the model regarding leakages will also be carried out to bring the model in a reliable shape and condition. Relevant data regarding pressures and temperatures will then be recorded and the pumping capacity of the model will also be tested to match the designed requirement. The working will also be recorded, and the oscillations will be analyzed in the Video Modeler and Analysis software. The model will also be tested with different composition of the working liquid by mixing water with an appropriate and available chemical for the sake of development of the fluidyne engine and the trends in the testing and experiments of the engine will be recorded and analyzed. The information and results gathered will then be validated with a model of the engine in the Computational Fluid Dynamics (CFD) Fluent Analysis.

3.1 Mathematical Equations

The theory research around fluidyne is all in attempt to develop a valid mathematical model for evaluating a fluidyne behavior. Stammers and West based on their research work have derived equations for this purpose but their indecisiveness and inapplicability in a dynamic oscillating system restrict their use. It is to note that a mathematical model for a loaded configuration of a fluidyne engine is an extremely complex task.

Recently, Turkish research group of Özdemir, Arslantürk, and Özüç derived applicable model with fair accordance to experimental values of an unloaded fluidyne engine.

Kyei-Manu and Obodoako in their paper demonstrated that for maximum amplitude of oscillation in liquid column, flow losses need to be minimized with frequency of the system

close to natural frequency for resonance to occur [15]. This is illustrated by U-tube form of displacer with assumption of both ends being open to atmosphere. Level is raised slightly in one arm of the tube by a distance x. One end of the liquid column now has more weight of liquid than the other, by an amount $2\chi A_d\rho$ where: χ = the amount by which the liquid is displaced; A_d = the cross-sectional area of the U-tube; ρ = density of the liquid.

This leads to the arise of pressure equal to $2\chi\rho g$ with g = acceleration due to gravity. Multiplying this term with area A_d resulting force is achieved equal to $2\chi A_d\rho$. The mass of the liquid column is $A_d\rho L_d$ (L_d being the length of the column) and so the acceleration induced by this force (in a direction to reduce χ) is given by

$$A_d\rho L_D\ddot{x} = -2xA_d\rho g \qquad \mathbf{2}$$

$$\ddot{x} = \frac{-2gx}{L_D} \qquad \mathbf{3}$$

The natural frequency for the liquid column is given by

$$\omega = \sqrt{\frac{2g}{L_D}}\,\mathrm{rad/s} \qquad \mathbf{4}$$

$$f = \frac{1}{2\pi}\sqrt{\frac{2g}{L_D}}\,\mathrm{Hz} \qquad \mathbf{5}$$

And the frequency for the tuning column is given by

$$f = {}^{1}/_{2\pi}\sqrt{\left(\frac{A_t P_m}{V_m\,\rho L_t} + \frac{\left[1+\frac{A_t}{2A_d}\right]g}{L_t}\right)}Hz \qquad \mathbf{6}$$

A_t is the tuning column cross-sectional area, L_t being length of the column, P_m initial gas pressure and V_m mid-stroke volume.

3.2 Design Calculations

Generally, the frequency of the Liquid Piston Stirling engine lies in the range 0.5-5 Hz. For our case, the engine is designed for a 1.5 Hz frequency value. Using the equation for the length of the displacer,

$$L_d = \frac{g}{2\pi^2 f^2} \quad \textbf{7}$$

$$L_d = 22.1\ cm$$

The engine should fulfill a pumping requirement of 0.5 m^3/hour through a 42.5 cm pumping arm length. The theoretical power output through this head is found out using,

$$P_o = \dot{V}\rho_w L_p \frac{g}{3600} \quad \textbf{8}$$

$\dot{V}$ is the volume flowrate, ρ_w is the density of water and L_p is the pumping arm length,

$$P_o = (0.5)(1000)(0.425)\frac{(9.81)}{3600} = 0.5790\ W.$$

As fluidyne machines efficiency exist around 4-6 %, the power input requirement is found taking efficiency of 5% as

$$P_{in} = \frac{P_o}{\eta} \quad \textbf{9}$$

$$P_{in} = 11.58 \sim 12\ W.$$

The swept volume can be found using the equation

$$P_o = B_n P f V_o \quad \textbf{10}$$

P_o being power output, B_n Beale number, P mean pressure (assumed as 1 atmospheric), f frequency and V_o (swept volume).

The Beale number may range from 0.15 to 0.11 for engines with high temperature differentials and may also be as low as 0.005 for very small temperature differentials. For our case, a value of 0.085 is taken to be as Beale number as the temperature differential of our design is not going to be of a very small temperature differential but also not of a very high-pressure differential.

$$V_o = \frac{0.5790}{(0.085)(1)(1.5)}$$

$$V_o = 4.5238\ cm^3$$

Proceeding by fixing the diameter of the pistons, the projected stroke, which is the amplitude of the oscillations can then be expressed as

$$V_o = \frac{s\pi(d_p)^2}{4} \qquad \textbf{11}$$

s being the stroke and d_p the diameter of the piston fixed as equal to 1.2 cm

$$s = \frac{4(4.5238)}{\pi(1.2)^2}$$

s = 4.01 cm

The volume rise in the tuning column is same as 4.5238 cm^3, the diameter of tuning column is fixed as 0.8 cm. Using this data, the amplitude of oscillations produced in tuning column can be found with

$$4.5238 = \left(\frac{\pi}{4}\right)(0.8)(amplitude\ of\ oscillation\ in\ tuning\ column)$$

Oscillation amplitude is found as 7.1998 ~7.2 cm.

The total volume of the working gas in cylinders is given by the equation

$$V_{gas} = 7V_o \qquad \textbf{12}$$

$$V_{gas} = (7)(4.5238) = 31.66 \text{ cm}^3$$

Again, for the portion of engine from cold to hot end to occupy this much volume of gas with diameter fixed as 0.9 cm the length of the portion (L_{wg}) can be found as

$$31.66 = (\frac{\pi}{4})(0.9^2)(L_{wg})$$

$$L_{wg} = 49.776 \sim 50 \ cm^3$$

To find the pumping line diameter, it is first important to determine the volume to be pumped per stroke to fulfil the pumping requirement of $0.5 m^3$/hour. For this purpose,

$$Strokes = f(3600) \qquad \textbf{13}$$

$$Strokes = (1.5)(3600) = 5400 \ strokes$$

$$Volume \ per \ stroke = \frac{0.5}{5400} = 92.6 \ cm^3/stroke$$

As the length of pumping line is known as 42.5 cm, diameter of pumping line is found as

$$92.6 = (\frac{\pi}{4})(d)^2(42.5)$$

$$d = 1.665 \sim 1.7 \ cm$$

- For the uniform flow and obeying the good practice of maintaining symmetry in fluidyne engines, the displacer region diameter is also kept as 0.9cm.
- Length of the tuning column is unrestricted if it supports the oscillations produced and maintains the liquid levels in the engine. For this reason, the length of that is kept as 75 cm.

4 Model Geometry

4.1 Basic Configuration Model:

Fluidyne engine comprises of liquid pistons which in this case is water. Model of fluidyne engine is overall rectangular shaped with copper pipe utilized in hot portion and the displacer portion that is bent to 90° between these two portions. The next bent part then connects with the transparent pipe of the cold end. Transparency of this pipe helps us to study the oscillations produced during operation. Also, the material used has enough melting point to sustain the heating introduced in the operation. Again, using the schematic of the model shown previously as well.

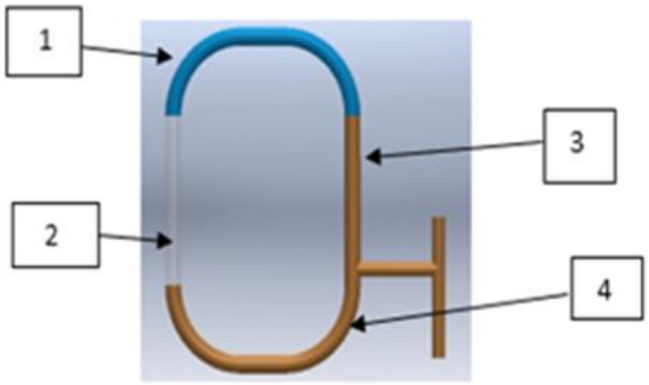

Figure 7. Schematic of Engine.

Table 1. Dimension of the model.

Section Number	Length	External Diameter	Internal Diameter
1-Connecting arm	40.6 cm	1.3 cm	0.65 cm
2-Transparent portion	20.3 cm	1.5 cm	1.3 cm
3- Hot end portion	30.5 cm	1.3 cm	1.3 cm
4- Displacer portion	15.2 cm	1.3 cm	1.3 cm

The choice of copper as the metal conductive pipe of its high thermal conductivity, low coefficient of expansion and high melting point as shown in the table 2

Table 2. Properties of Copper.

Thermal conductivity (W/cm°C) at 20°C	3.94
Melting point (°C)	1083
Coefficient of expansion (°C-1)	17 x 10-6

In the assembly of the model instead of using joints at the ends of displacer the pipe is bent to 90 degrees. Similarly, instead of using a T-joint to connect output column with hot end a copper pipe of 3/8 inch is joined by welding after drilling a hole in the hot column pipe. This pipe is further welded to another pipe of 0.375 inch which then connects with output column of diameter 0.375 inch through a union.

Figure 8. Constructed basic configuration hand model of fluidyne.

4.2 Improvised Model:

After the first model, a second model was constructed to improve and enhance the working of the first model. The first model with its flaws of leakage, burnt/melted pipes, loose and broken valves

made it complicated to conduct a working experiment with feasible results. It was then improved with better equipment at hand and with prior knowledge, an improved and working model was first designed on CAD software and then constructed as shown.

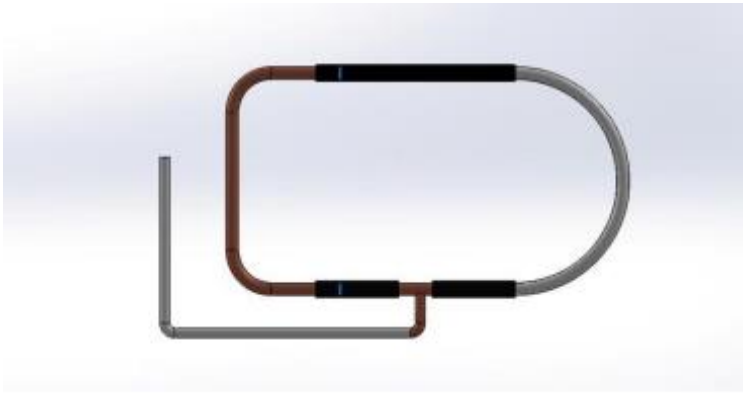

Figure 9. CAD model of the improvised model.

Material choice is still Copper as in the previous model but some changes to the dimensions were made.

Table 3. Dimensions of the improvised model.

Section Number	Length	External Diameter	Internal Diameter
1-Regenerator	33 cm	1.3 cm	0.65 cm
2- Cold End Portion	38.1 cm	1.5 cm	1.3 cm
3- Hot End Portion	22.9 cm	1.3 cm	1.3 cm
4- Displacer Portion	33 cm	1.3 cm	0.5 in

Figure 10. Constructed improvised model.

Additional apparatus was also made use of in the testing of this improvised model which included different sensors, connection and techniques.

Vernier Gas Pressure Sensor was used to measure the pressure variations. It has a pressure range from 0 kPa to 210 kPa (0 to 2.1 atm) with an accuracy of 4Kpa. The maximum it can tolerate with damage is 405 kPa.

Figure 11. Vernier Pressure sensor.

Vernier Surface Temperature Sensor was used to measure the temperature variations. It has a range from -25 C° to 125 C° (-13 F° to 257 F°) with an accuracy of 0.5 C°. The maximum it can tolerate with damage is 150 C°.

Figure 12. Vernier Surface temperature sensor used in testing; the white tip of the sensor was introduced to the testing area.

For the integration of the sensors Arduino setup was utilized. The Arduino connection was made with the breadboard using jumper wires while code was loaded in the laptop using the installed Arduino IDE. Wiring procedure was aided from the vernier user manuals. Using the instructions provided by Vernier sketches, the Protoboard adapter was connected to the breadboard. It included six labelled pins and were connected as described.

- Wiring a Single Digital Protoboard Adapter: DIO0 (Vernier BTD pin 1) to Arduino pin 2 (function depends on sensor)
- DIO1 (Vernier BTD pin 2) to Arduino pin 3 (function depends on sensor)
- DIO2 (Vernier BTD pin 3) to Arduino pin 4 (function depends on sensor)
- 5V (Vernier BTD pin 4) to Arduino pin 5V (power)
- GND (Vernier BTD pin 5) to Arduino pin GND (ground)
- DIO3 (Vernier BTD pin 6) to Arduino pin 5 (function depends on sensor)

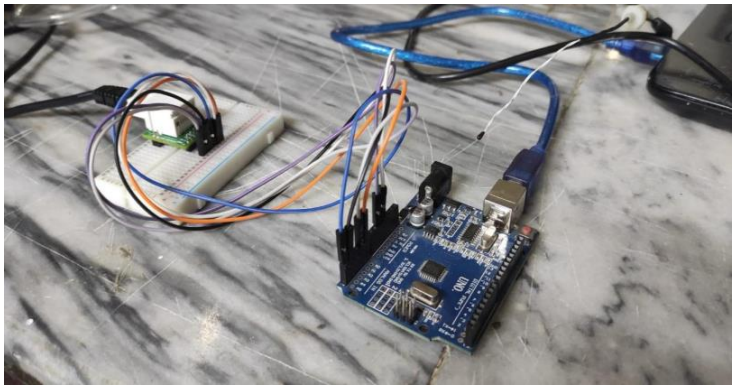

Figure 13. Arduino setup for sensors integration.

```
#include "VernierLib.h" //include Vernier functions in this sketch
VernierLib Vernier; //create an instance of the VernierLib library
float sensorReading; //create global variable to store sensor reading
void setup() {
  Serial.begin(9600); //setup communication to display
  Vernier.autoID(); //identify the sensor being used
}
void loop() {
  sensorReading = Vernier.readSensor(); //read one data value
  Serial.print(sensorReading); //print data value
  Serial.print(" "); //print a space
  Serial.println(Vernier.sensorUnits()); //print units and skip to next line
  delay(500); //wait half second
}
```

Code used for the integration of the sensors using Vernier library and functions

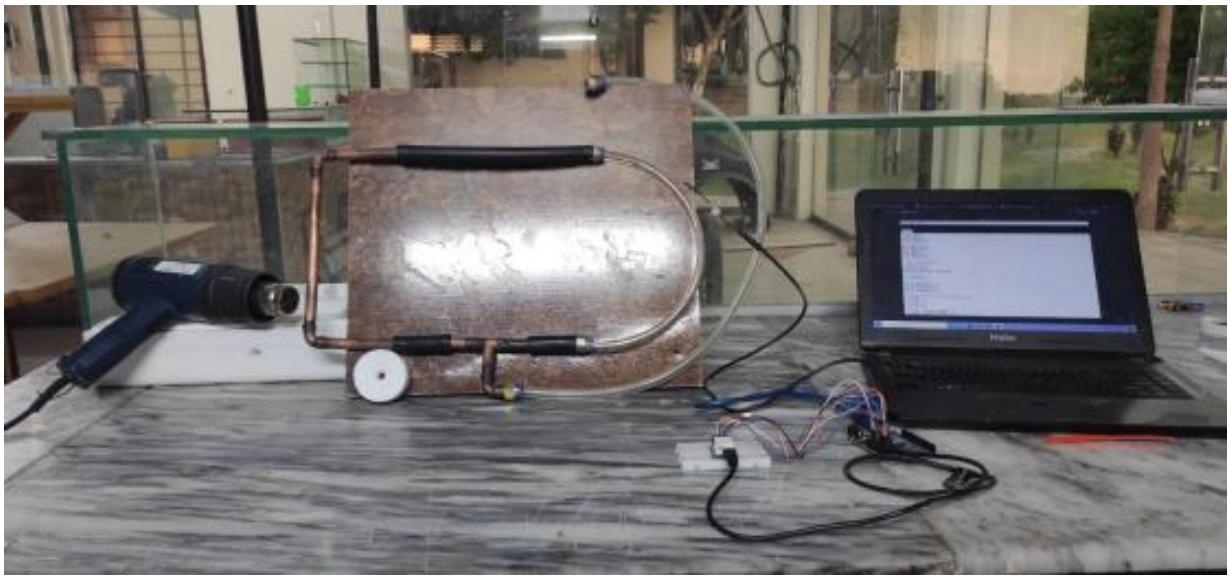

Figure 14. Entire Model Setup.

5 Analysis

5.1 Basic Configuration Model:

The output column and the cold end column of the fluidyne model are analyzed. As heat source a hot air gun is utilized with variable power outputs of 1000 W at position I and 2000 W at position II. Rated air temperature and flowrate at position I is 350°C and 300L/min and at position II is 600°C and 500L/min. For analyzation of the columns video tracker software Logger Pro 3 is utilized. Recorded videos were uploaded on the software. For the 1000 W power with gun at 4 cm, the following graphs of displacement and velocity of the oscillations of water level in output column and the cold end column were plotted in the software.

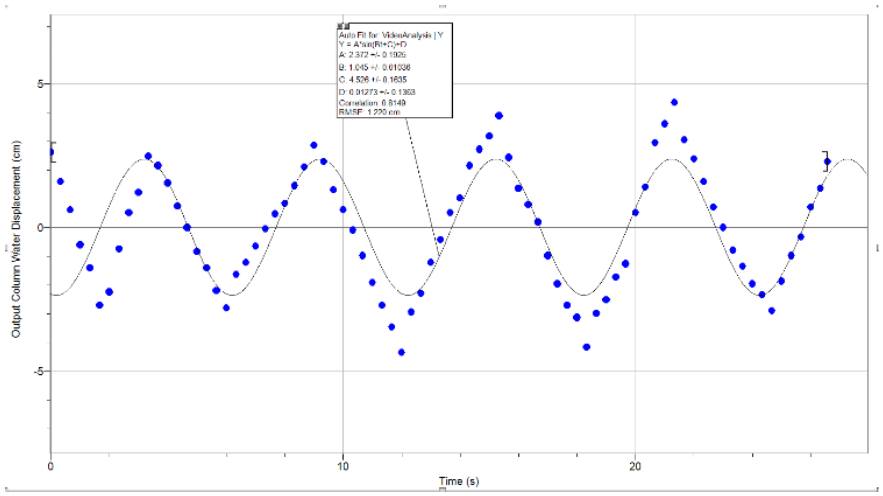

Figure 15. Amplitude vs Time Graph. The maximum amplitude plotted is 4.3 cm.

From graph parameters calculated were:

Peak-1 = 2.5cm Peak-2=-2.5cm

D = Peak-1 - Peak-2=5cm, Time Period =6.25sec & Frequency = 0.16Hz

Due to and fro motion about mean position. Amplitude of oscillation vs time follows a sine curve.

Mathematically,

$$A = \frac{D*sin(2\pi ft)}{2} \quad \textbf{13}$$

Here, D= Peak-to-Peak Value and A = Amplitude

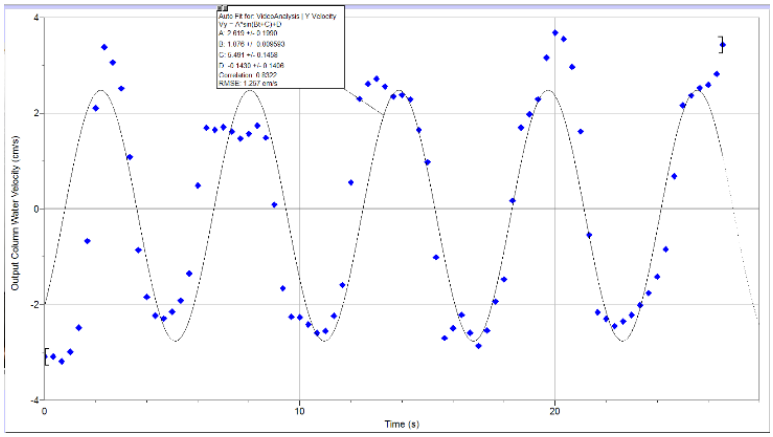

Figure 16. Velocity vs Time Graph. The maximum velocity plotted is 3.7 cm/s.

Mathematically, velocity graph follows following relation.

$$V = \pi f*D*cos(2\pi ft) \quad \textbf{14}$$

Here, V = velocity in cm/s.

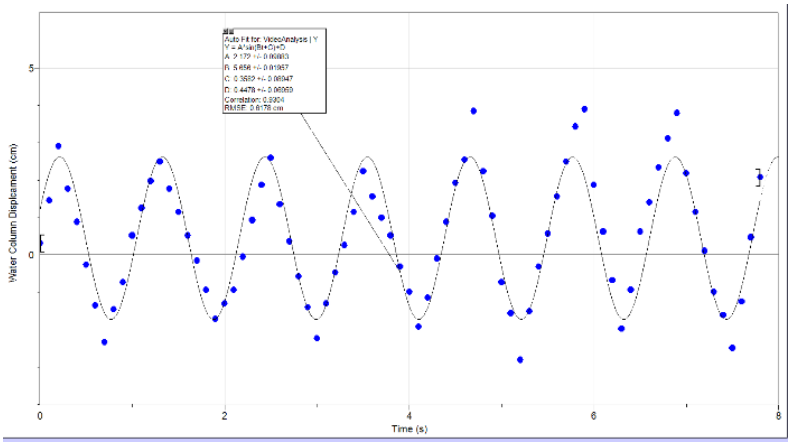

Figure 17. Amplitude of the oscillations for the best fit curve in the tuning column (varies from 2.5 cm to 1.5 cm, the maximum amplitude plotted is around 3.9 cm).

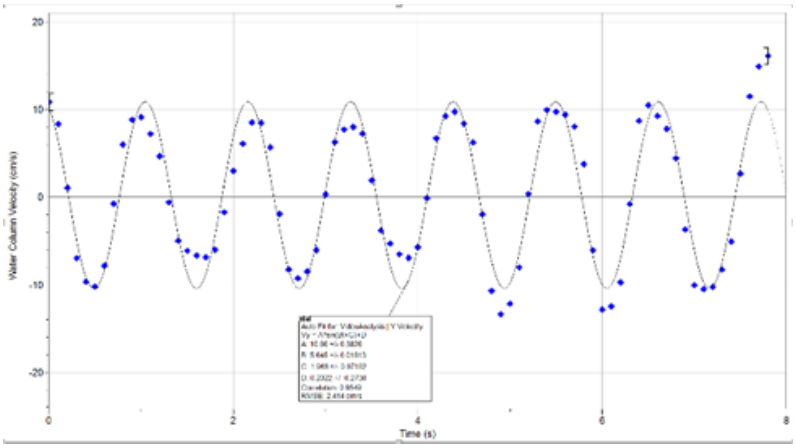

Figure 18. The maximum velocity of water for best fit curve is 10 cm/s in the oscillations in the tuning column.

Similar graphs for the tuning and cold end column are plotted for the position II of the hot air gun.

The hot air gun is placed at the same distance from the hot end. The graphs are shown below.

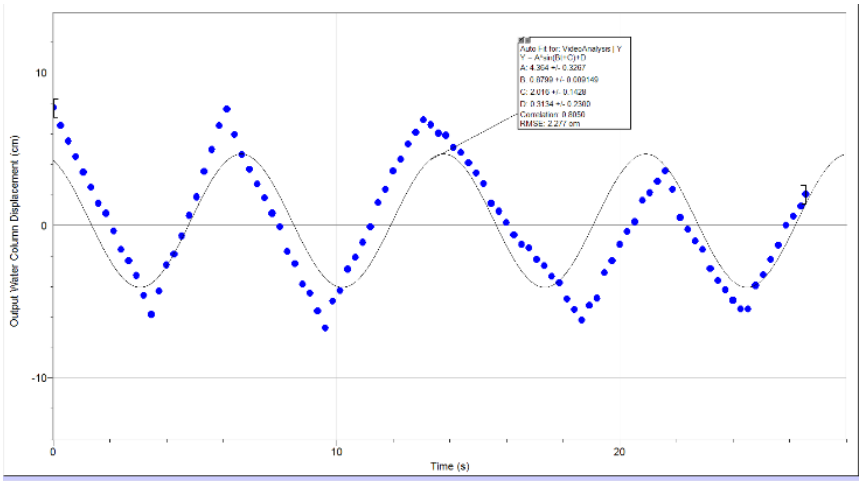

Figure 19. Amplitude vs Time Graph. The maximum amplitude plotted is 8 cm.

From Graph following parameters have been calculated:

Peak-1 = 4.5cm Peak-2=-5.8cm

D = Peak-1 - Peak-2=10.3cm, Time Period =7.5sec & Frequency = 0.13Hz.

Again, it is concluded that the amplitude as function of time follows following relation.

$$A = \frac{D*sin(2\pi ft)}{2}$$,D= Peak-to-Peak Value & A = Amplitude

Similarly, by tracker software velocity and time graph has been plotted.

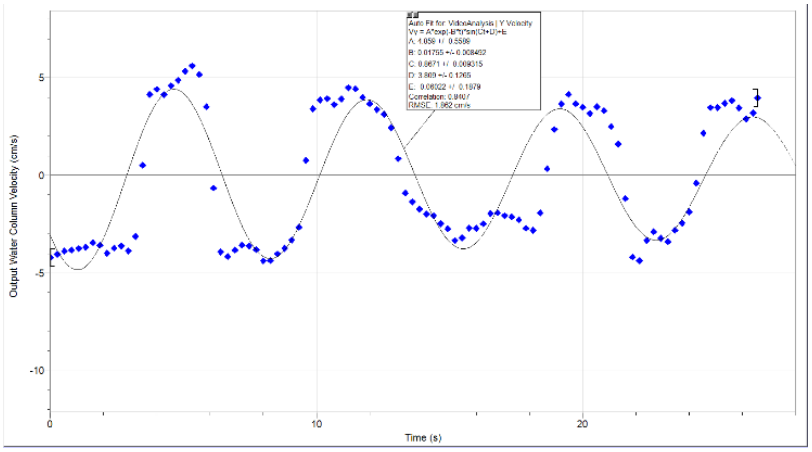

Figure 20. The maximum velocity of water for best fit curve is around 4cm/s in the oscillations in the cold end column. The maximum velocity plotted is 6 cm/s.

Mathematical equation relating parameters.

$$V = \pi f * D\cos(2\pi f t),$$ V = velocity in cm/s.

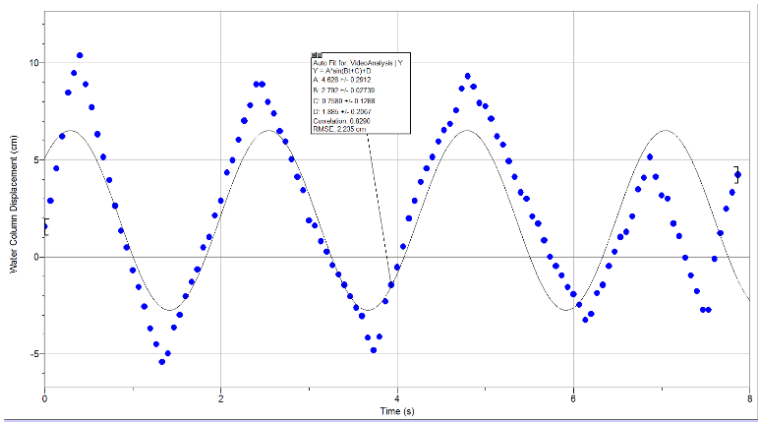

Figure 21. Amplitude of the oscillations for the best fit curve in the tuning column is 6.5cm. The maximum amplitude plotted is around 10.8 cm.

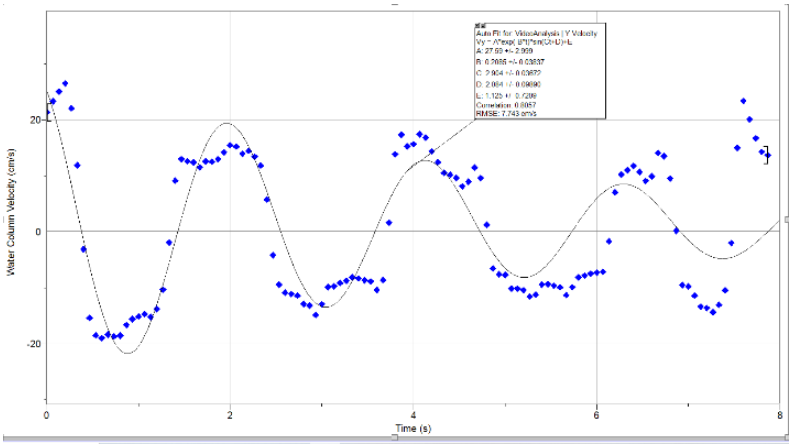

Figure 22. The maximum velocity of water for best fit curve is around 15 cm/s in the oscillations in the tuning column. The maximum velocity plotted is 25cm/s.

5.2 Improvised Model:

The heating environment and the use of the hot air gun was carried out in the same way as in the previous model for 2000 W. The testing strategy in the improvised model included testing for effects of volume of the working fluid in the engine and the liquid column vaporization on the pressure, temperature and oscillations amplitude and stability trends of the engine.

5.2.1 Effects of Working Liquid Volume

To better understand the contributions that volume of the working liquid in engine has on its performance, a variety of tests were carried out. In these tests volume of the working liquid which is water in our case was varied as 100 ml and 80 ml (1ml equals 0.000001 cubic meter). The effects of the varied volumes were studied in respect to oscillations amplitude and stability, pressure and temperature variations in the cold end, and the pumping power at that volume

Testing method includes inserting the transducer portion of the Vernier gas pressure and temperature sensors through a small hole in the cold end portion of the engine. The sensors are connected to Arduino UNO board via a connector which is then integrated with a laptop. Leakages through hole does not occur due to sensor arrangement. The volumes of water are inserted using a syringe in the engine. To measure the pumping capacity of the configuration a 30 ml test tube was placed at the outlet of the pumping line, the volume pumped was measured against a stopwatch. The readings of the temperatures and pressure recorded in Arduino IDE were next plotted on Excel.

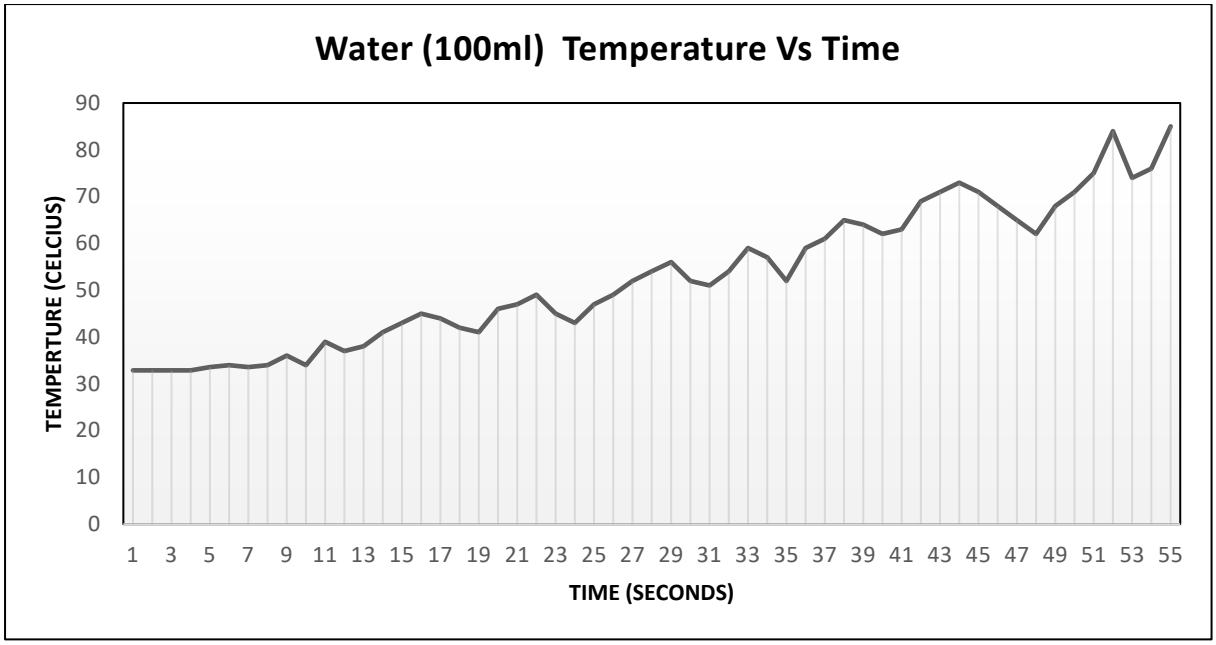

Figure 23. Temperature vs time curve for pure water in engine with 100 ml volume

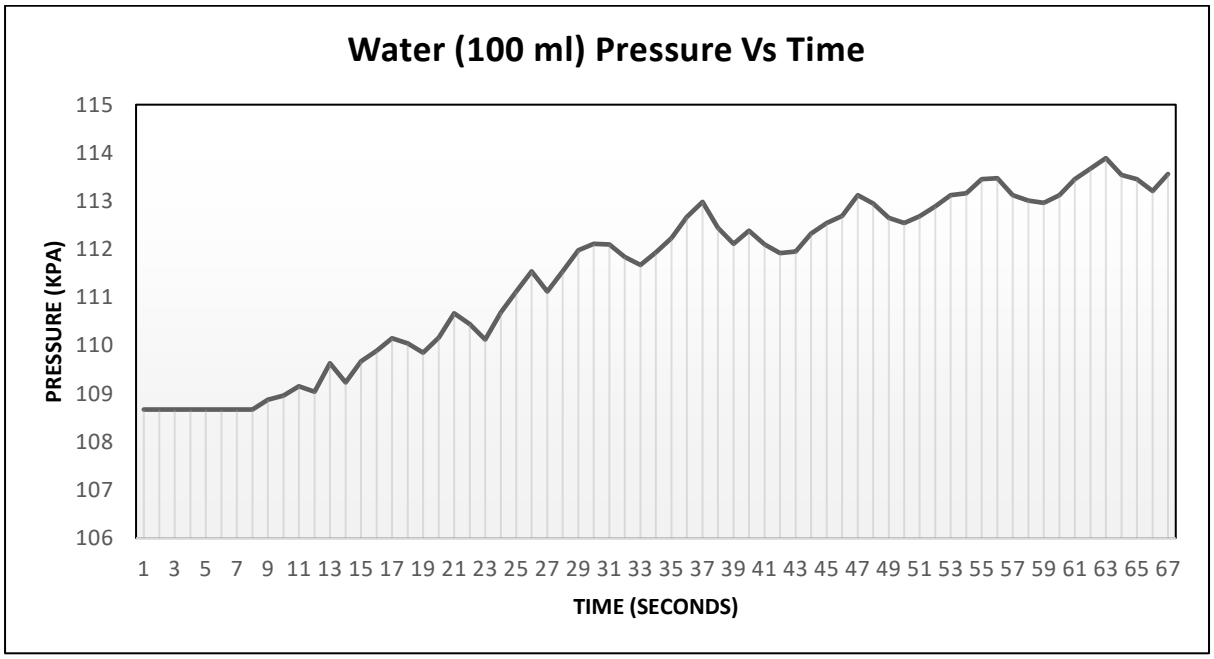

Figure 24. Pressure vs time curve for pure 100ml water in the engine

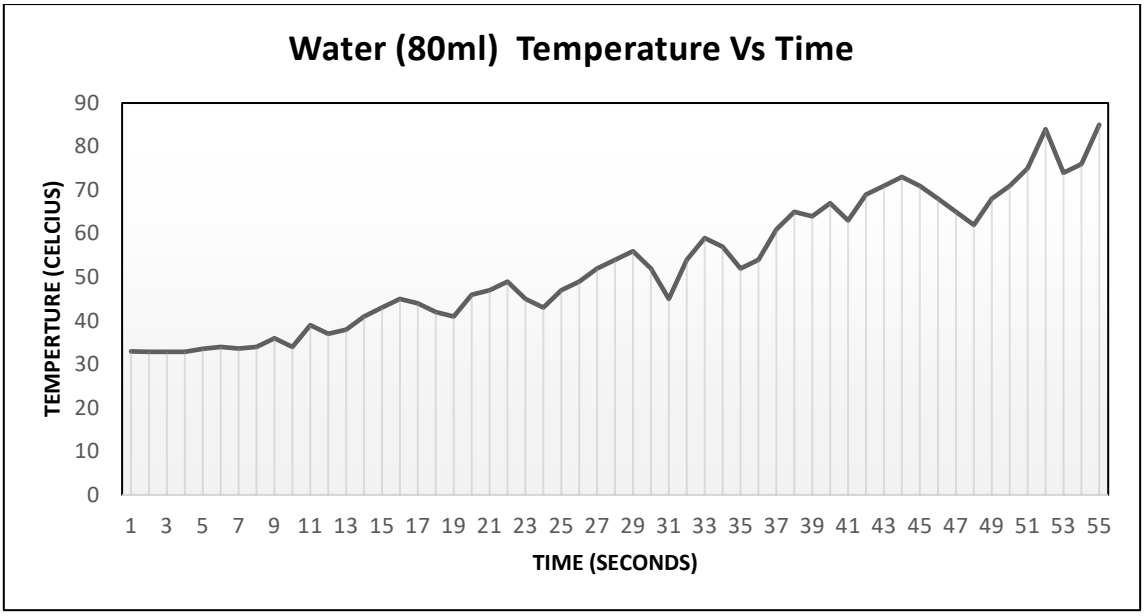

Figure 25. Temperature vs time curve for pure water in engine with 80 ml volume

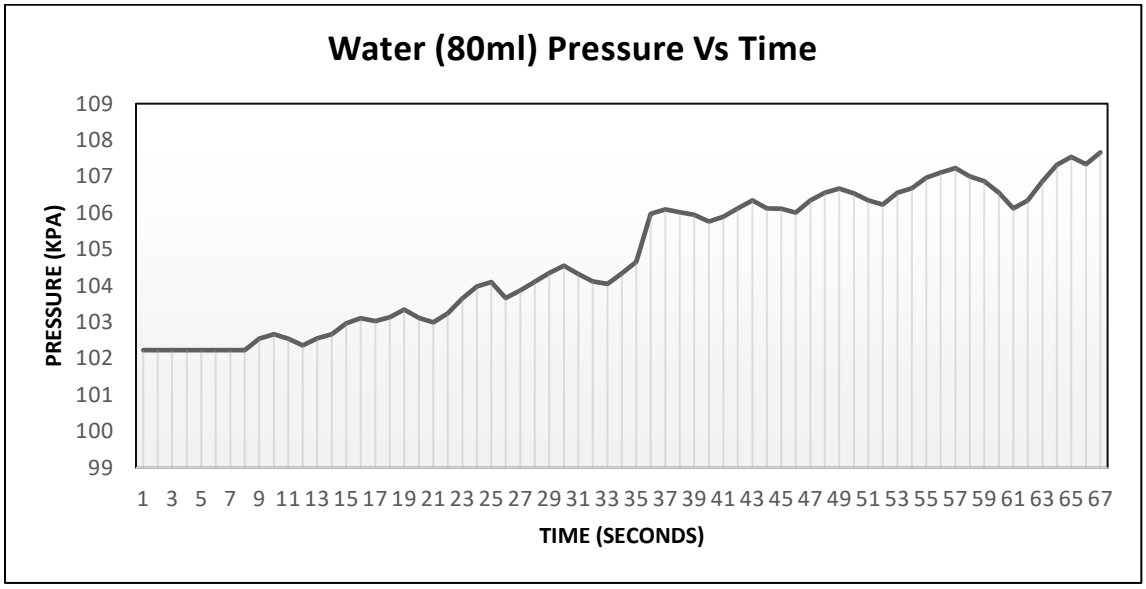

Figure 26. Pressure vs time curve for pure water in engine with 100 ml volume

The analyzation of the graphs showed that the temperature variations for the cold end remained similar in both 80ml and 100ml working fluid volume. This is strongly reasoned and implied by the constant heat input to the hot end in the system. The pressure variations for the 100ml volume case lied in the range 108-114 kPa while for the 80 ml volume case the variation majorly existed between 102-107 kPa. This implies that although the pressure varied by equal

values in the cold end the magnitude of the pressure trend in the cold end for the 100 ml case is more than the 80 ml case. This is also reflected and supported by the pumping data regarding both cases.

The next part the analysis for these volumes included graphs for the oscillations produced in the tuning column, for which the recordings of the oscillations were uploaded on the Video Modeller and Analysis Software. For a clear observation the origin was selected as the stagnant liquid level in the tuning column and liquid being observed by default settings of the software were under the name of mass A.

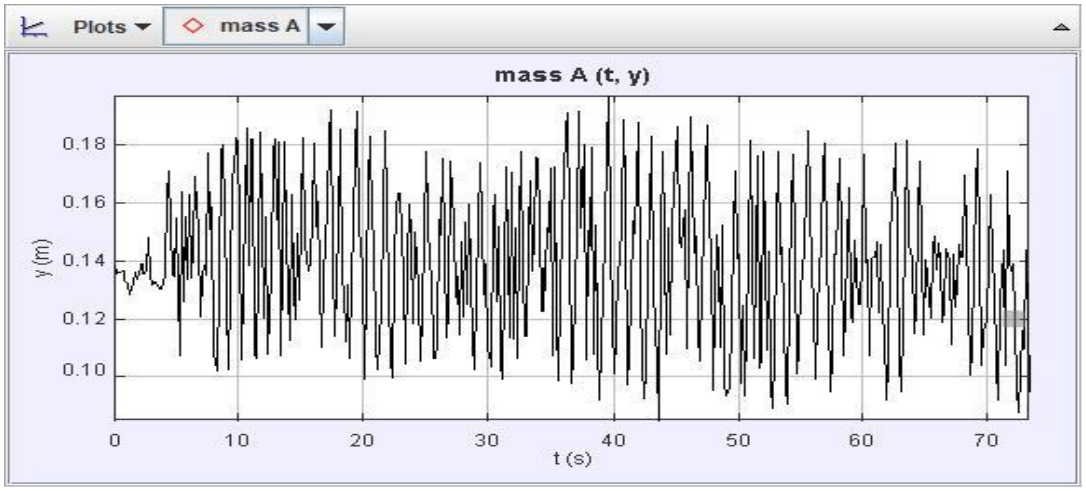

Figure 27. Oscillation amplitude vs time curve for pure water with 100 ml volume in tuning column

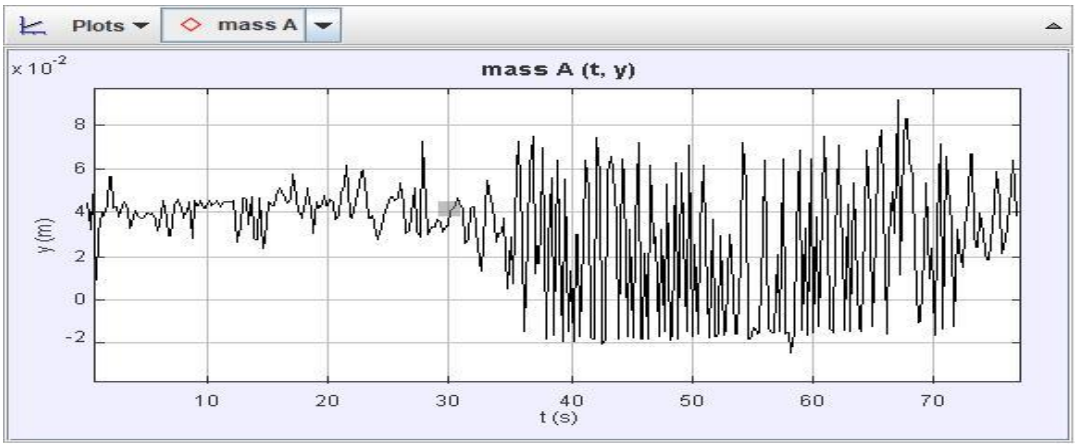

Figure 28. Oscillation amplitude vs time curve for pure water with 100 ml volume in tuning column

Analysing the graphs of the oscillations in the tuning column showed that the frequency of these oscillations for both cases were similar however, for the case of 100 ml the amplitudes are higher with respect to the 80 ml oscillations. The frequency of the oscillations remained a factor of engines geometry and heat input.

Table 4. Pumping data for different working fluid volume cases

Working Liquid Volumes /ml	Pumped Volume (measured from the point of start of pumping) / ml	Time Taken/s
100	20	22
80	8	25

The data showed that at more volume of water in the engine the pumping was achieved sooner and at a higher rate as when it was less. The pumped volume of water was received in a 20 ml test tube and observed for shorter time periods.

This data also varied by the designed data, the engine was designed to pump 0.5 cubic meter per hour but the maximum it pumped with 100 ml liquid in it 0.91 ml/sec (0.00328 cubic meter/hour) this only 0.656 % of what was intended but understandable given that the fluidyne engines are known for their low efficiency and the frictional power losses were not considered in the calculations.

5.2.2 Effects of Liquid Column Vaporization

The next part of the research is to notice the effects on engine performance by the vaporization of liquid pistons. For this purpose, an alcohol that is Ethylene Glycol is used to achieve variations of vapor pressure to understand how fluid vaporization is related to engine

performance. The fluids were mixed volumetrically, and vapor pressure was calculated through Raoult's law.

From Raoult's law,

$$P_{solution} = X_{solvent} . P_{solvent} \quad \textbf{15}$$

$$X_A = \frac{n_A}{n_A + n_B} \quad \textbf{16}$$

Table 5. Heats of Vaporization and Vapor Pressure at 100 °C for working liquids

Liquid	Heat of Vaporization (kJ/mol)	Vapor Pressure @ 100°C
Water	40.66	87726
Ethylene Glycol	65.60	2466

Table 6. Composition and Vapor Pressure of the mixtures utilized.

Mixtures	Ratio (ml-ml) (vol. – vol.)	Vapor Pressure @ 100°C
Glycol, Water	20 – 80	70180
Glycol, Water	40 – 40	43863
Glycol, Water	50 – 10	14621

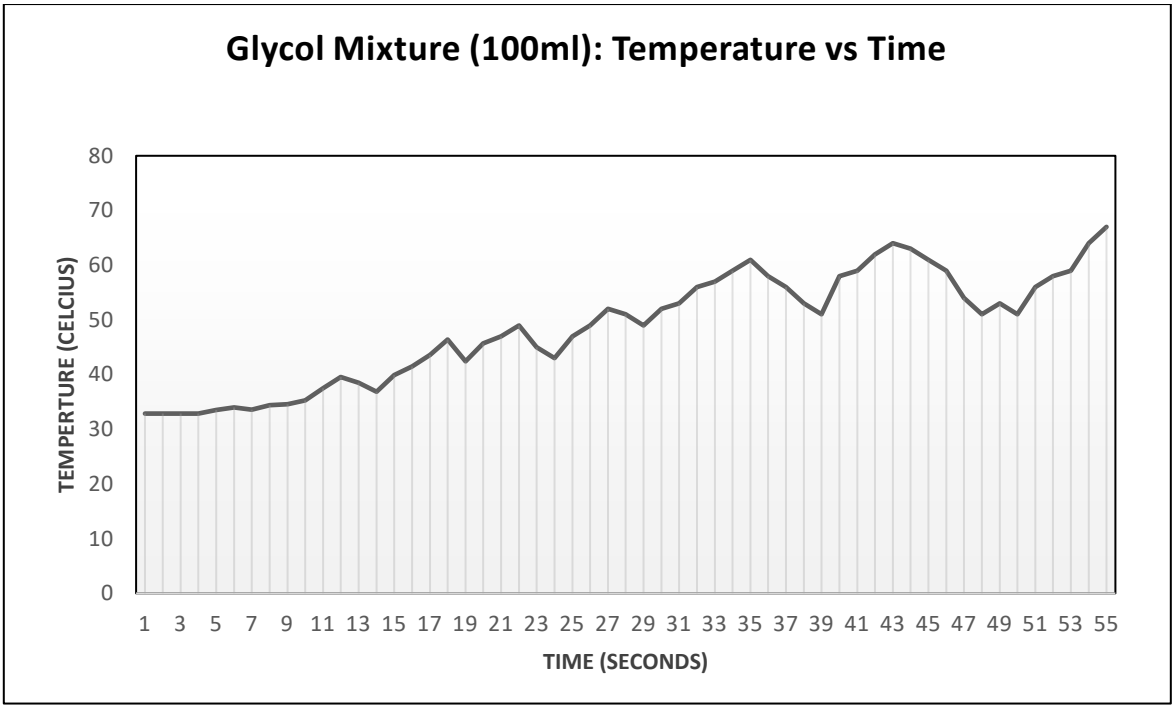

Figure 29. Temperature vs time curve for 100ml glycol mixture in engine

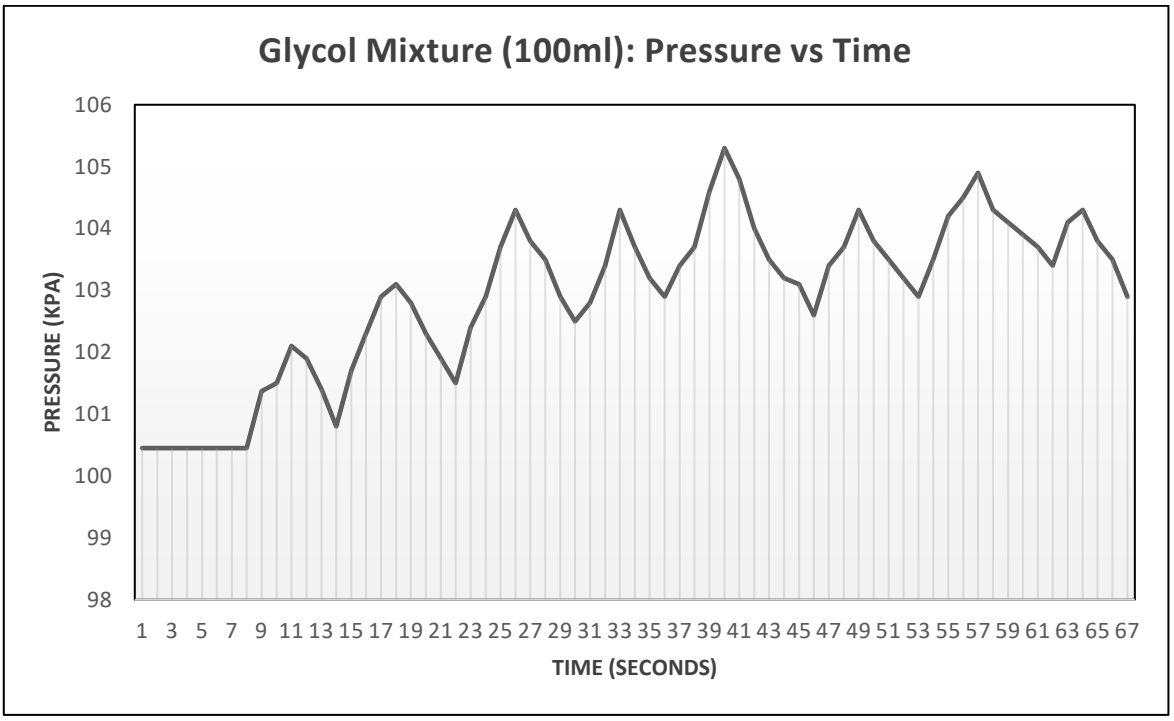

Figure 30. Pressure vs time curve for 100ml glycol mixture in engine

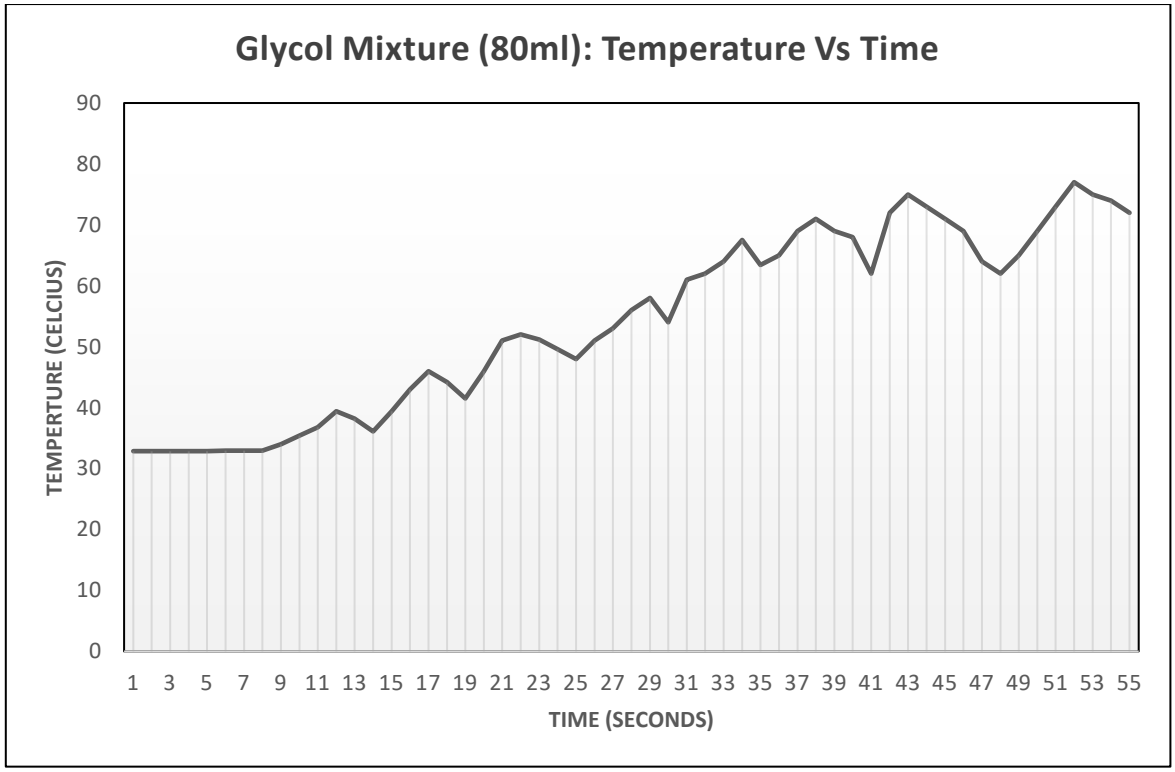

Figure 31. Temperature vs time curve for pure water in engine with 80 ml volume

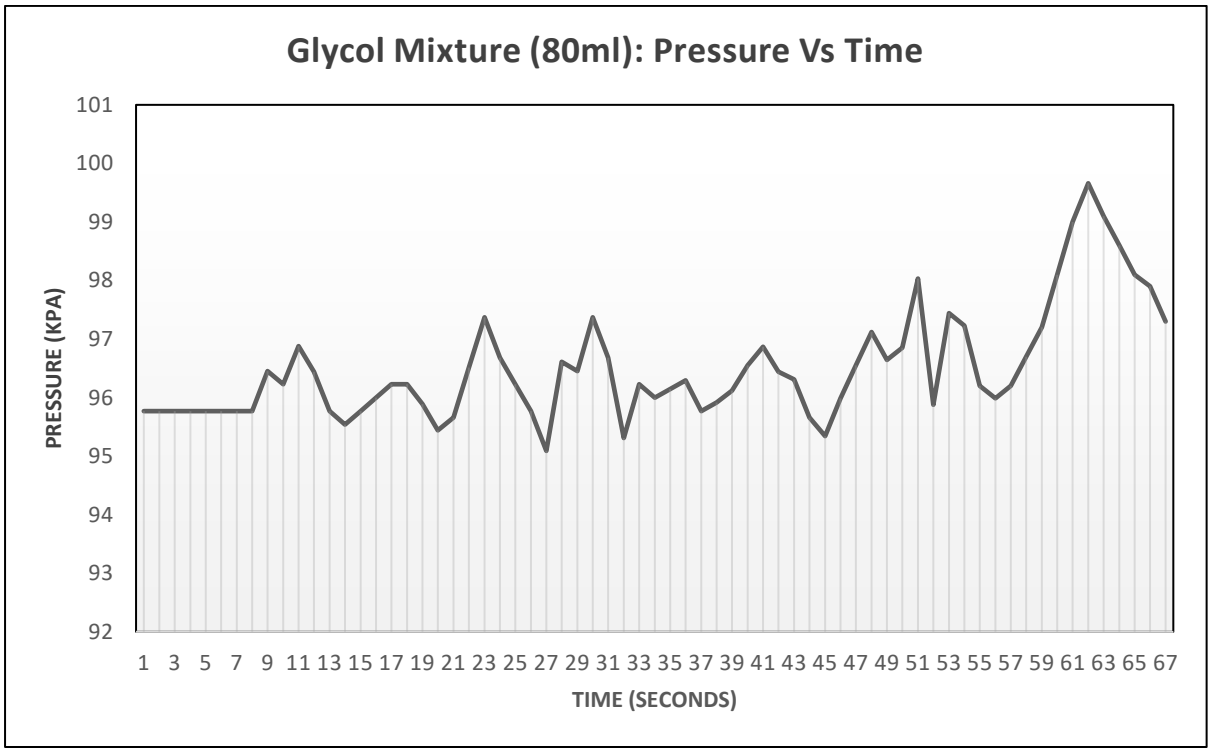

Figure 32. Pressure vs time curve for 80ml glycol mixture in engine

Due to the similar trends of temperature readings these are not plotted again for the 60 ml mixture.

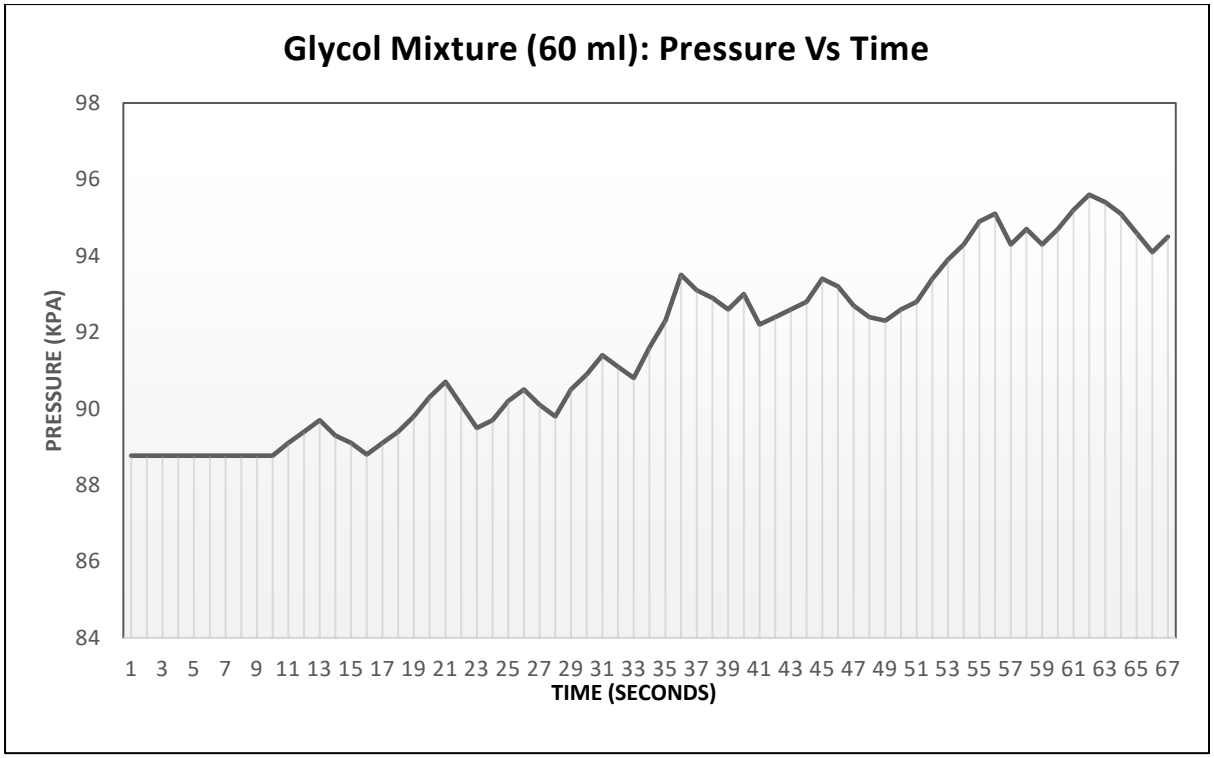

Figure 33. Pressure vs time curve for 60ml glycol mixture in engine

The oscillations produced in all three of the mixtures were recorded using a camera. These recordings were then used to analyse amplitudes and stability of the oscillations. The recordings of the oscillations were uploaded on the Video Modeller and Analysis Software. For a clear observation the origin was selected as the stagnant liquid level in the tuning column and liquid being observed by default settings of the software were under the name of mass A.

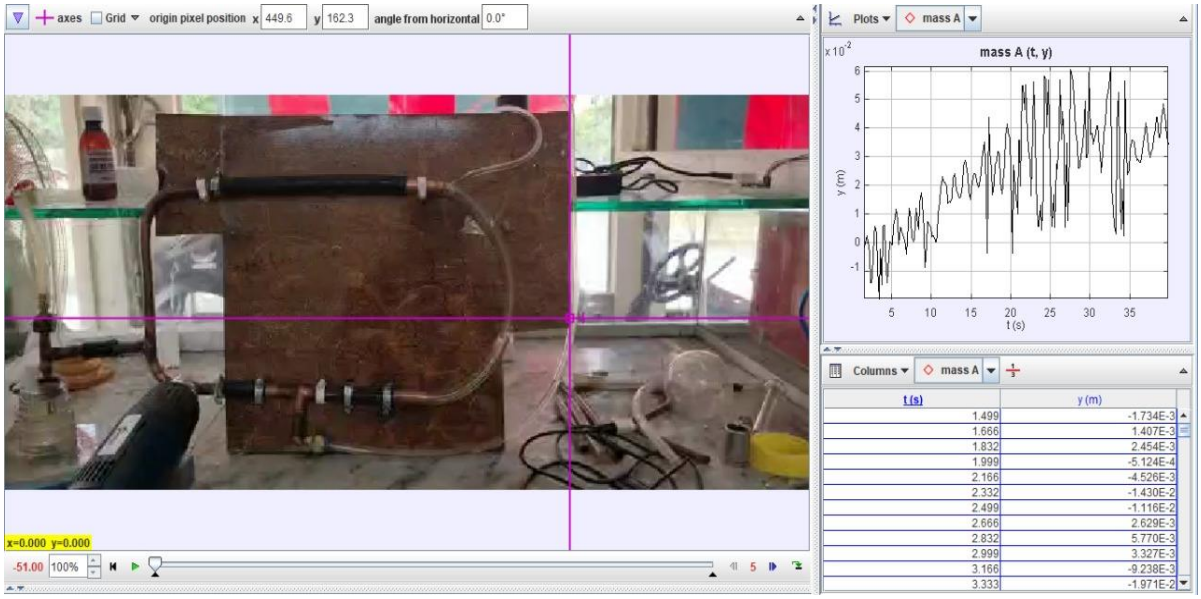

Figure 34. Video uploading on Video Modeler and Analysis software for 100 ml mixture

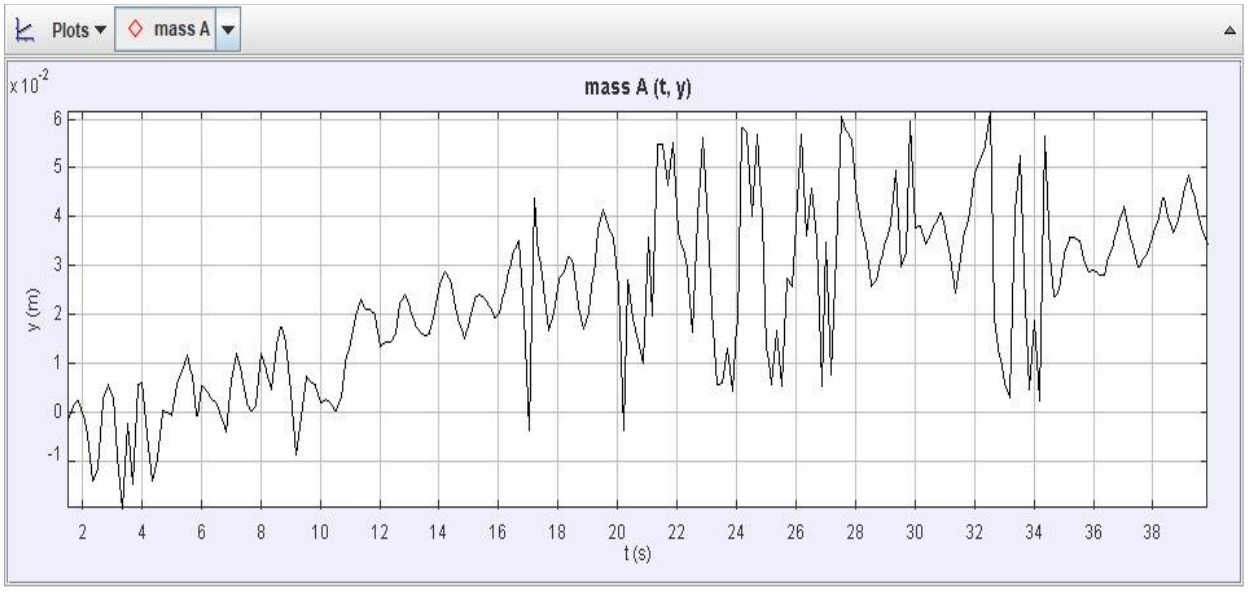

Figure 35. Amplitude vs time graph for 100 ml mixture

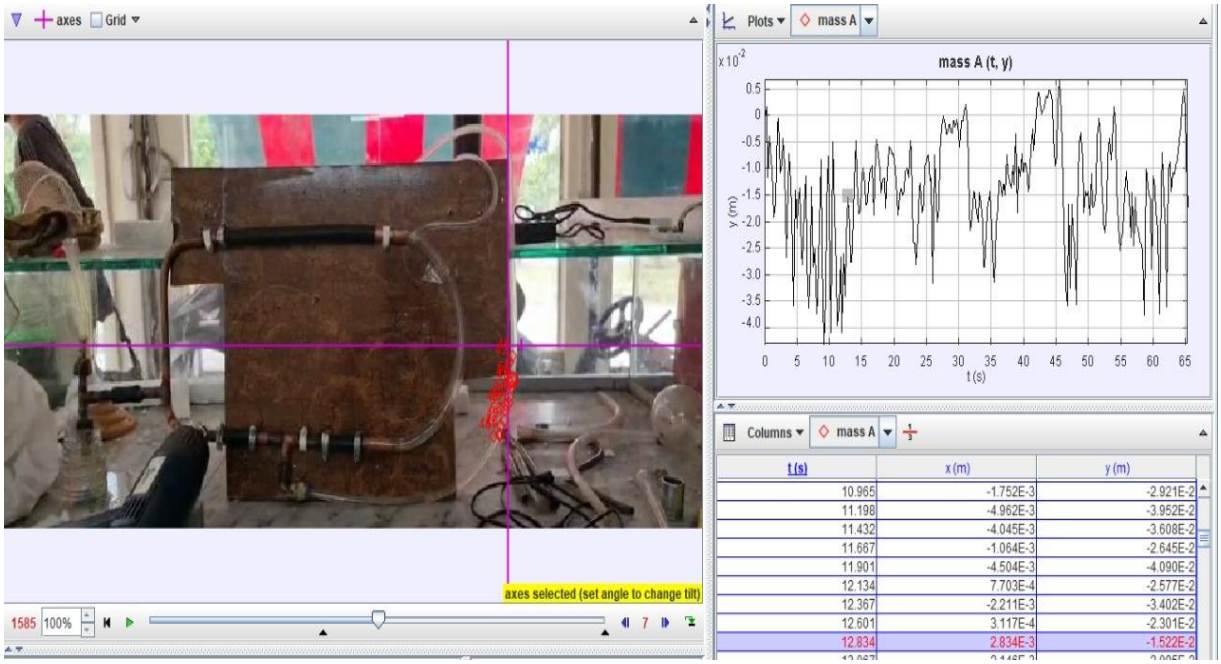

Figure 36. Video uploading on Video Modeler and Analysis software for 80 ml mixture

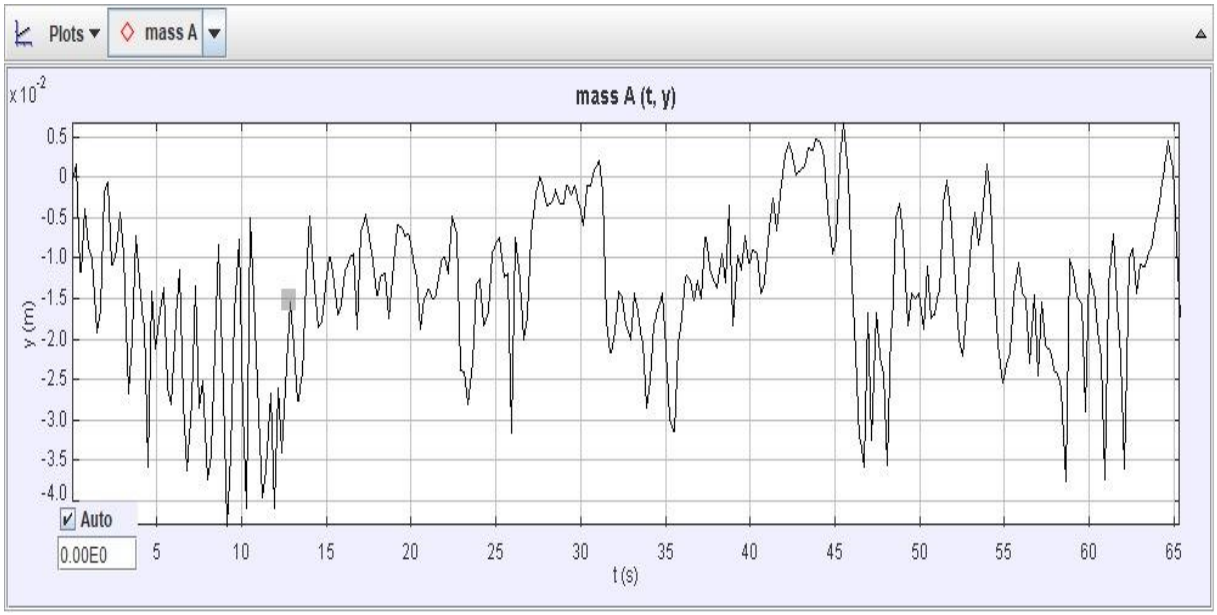

Figure 37. Amplitude vs time graph for 80 ml mixture

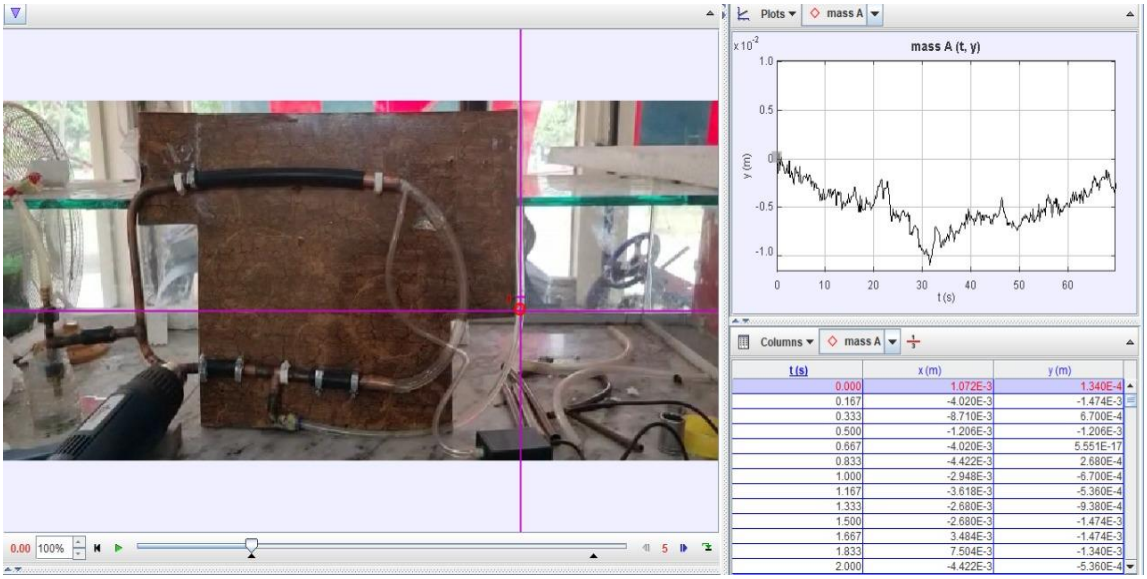

Figure 38. Video uploading on Video Modeler and Analysis software for 60 ml mixture

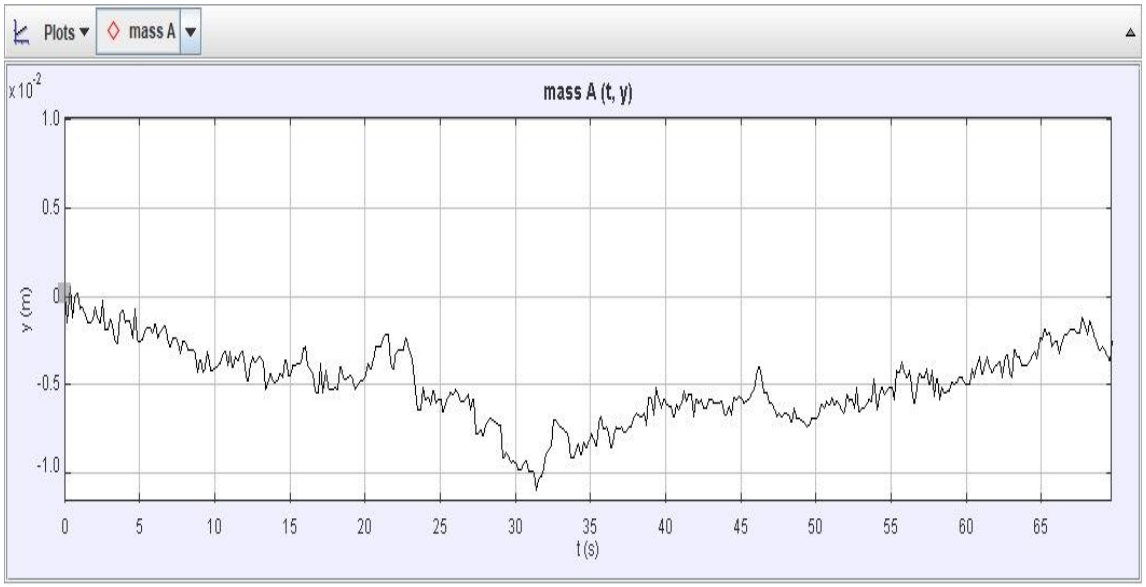

Figure 39. Amplitude vs time graph for 60 ml mixture

In all the cases the source of heat input and conditions were kept same, experimental results show that the range of pressure variation although is same, higher pressures are achieved with greater concentration of water than ethylene glycol. The temperature plots do not show a recognizable or definite trend possibly since heat input is maintained constant. The analyzation of amplitude vs time graphs from Logger 3 Pro software exhibit that when the

liquid columns are occupied with greater concentration of liquid with higher heat of vaporization the oscillations are somewhat more stable but with much smaller amplitude as compared to the mixtures with greater concentration of water in liquid columns demonstrate that liquids with a lower enthalpy of vaporization produce a greater amplitude of oscillation due to the higher conversion rate of input energy into vaporization at a given hot column temperature. It was observed that the engine's operational frequency is geometry dependent and independent of input energy back when the working liquid was just water however, testing indicated that some dependence of engine's operational frequency on the composition of glycol mixtures. This behavior is not further explored but there's strong reason that due to the significantly high viscosity of ethylene glycol as compared to water, there is likely some effect on the physical properties and hence the observed frequency change.

It is concluded with the indication of the results that as concentration of the lower heat of vaporization liquid increases, more energy can be converted to mechanical work and there is a strong correlation with power output of the engine and a high vapor pressure of the working liquid, for a constant temperature heat source. This is in congruency with results found by work performed by Markide's group in London which tested working fluids for a mechanical two-phase engine [16].

5.2.3 Computational Fluid Dynamics Model

For the analysis of the model, initially it was considered to be half filled with water with no inlet and outlet. Constant wall temperature input is applied at hot below wall and hot above wall. The cold end was maintained at constant temperature while other walls remained adiabatic.

For analysis 2D geometry was created In SolidWorks considering computational power. Liquid Piston Stirling Engine was divided into 4 regions hot end, cold end, regenerator, and

displacer. However, for this analysis the model was divided into 7 regions named as hot below, hot above, cold below, cold above, regenerator, displacer and open using split command to patch water, vapor region during initialization. Model was imported to Ansys Fluent in .STEP format.

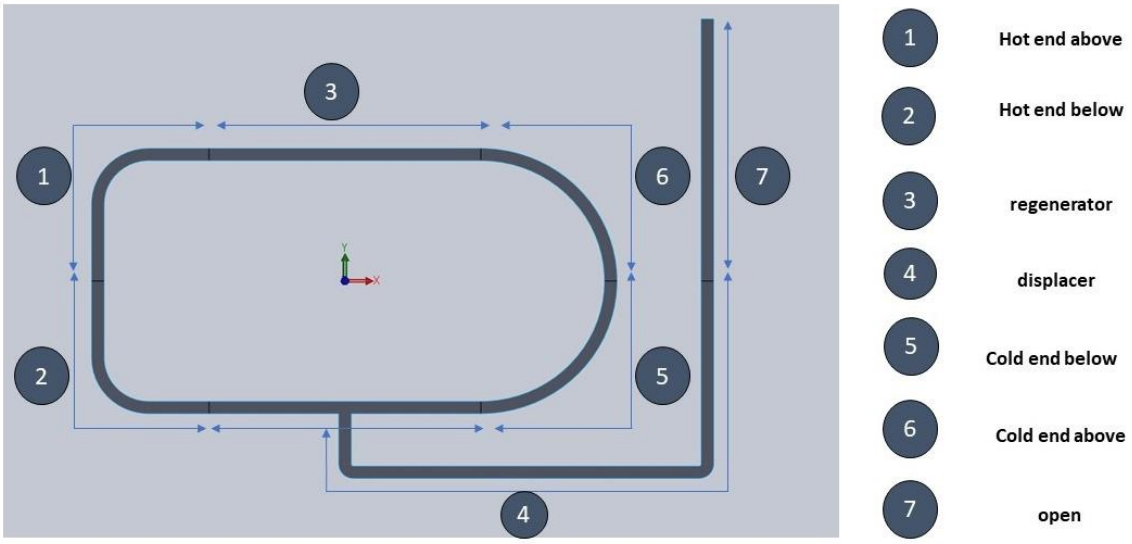

Figure 40. Division into different regions

5.2.3.1 Mesh Generation

Liquid Piston Stirling Engine during operation involves three fluids liquid, vapor and air. For capturing evaporation condensation phenomenon which takes place during engine operation, mesh must be fine, otherwise this phenomenon cannot be captured. Face Meshing was enabled to have smooth mesh across edges and faces. However increasing mesh size results in smaller time step size selection and results in more computational cost. To keep balance mesh independence was applied.

5.2.3.2 Mesh Independence

Initially element size was 0.001 and time step size was kept 0.001. Any timestep greater than 0.001 solution started to diverge. For element size of 0.004 mesh was coarse and at time step size of 0.01 solution convergence however results were slightly away from element size of 0.

001.Finally element size was set to 0.003 resulting mesh was fine and at time step size of 0.01 solution convergence. This is further explained below in Table 7, Table 8 and Table 9.

Table 7. Sizing details for element of size 0.001 (Case 1)

Element size:	0.001
Element Type:	Quadrilaterals
Number of Nodes:	20713
Number of Element:	18830
Mesh Quality:	Fine
Time step size	0.001
Computational Cost:	High

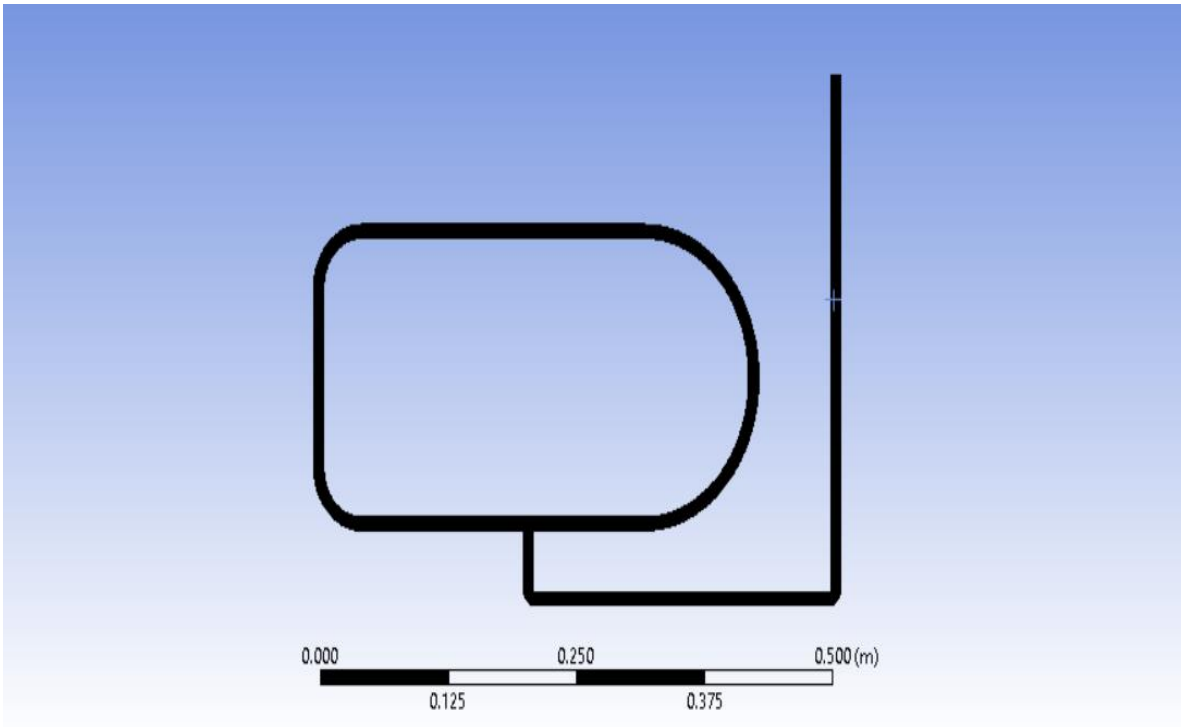

Figure 41. Mesh display Element size 0.001

Table 8. Sizing details for element of size 0.004

Element size:	0.004
Element Type:	Quadrilaterals
Number of Nodes:	1952
Number of Element:	1464
Time step size	0.01
Mesh Quality:	Fine
Computational Cost:	Low compared to case 1
Results:	Differ from actual physics of the problem and case 1.

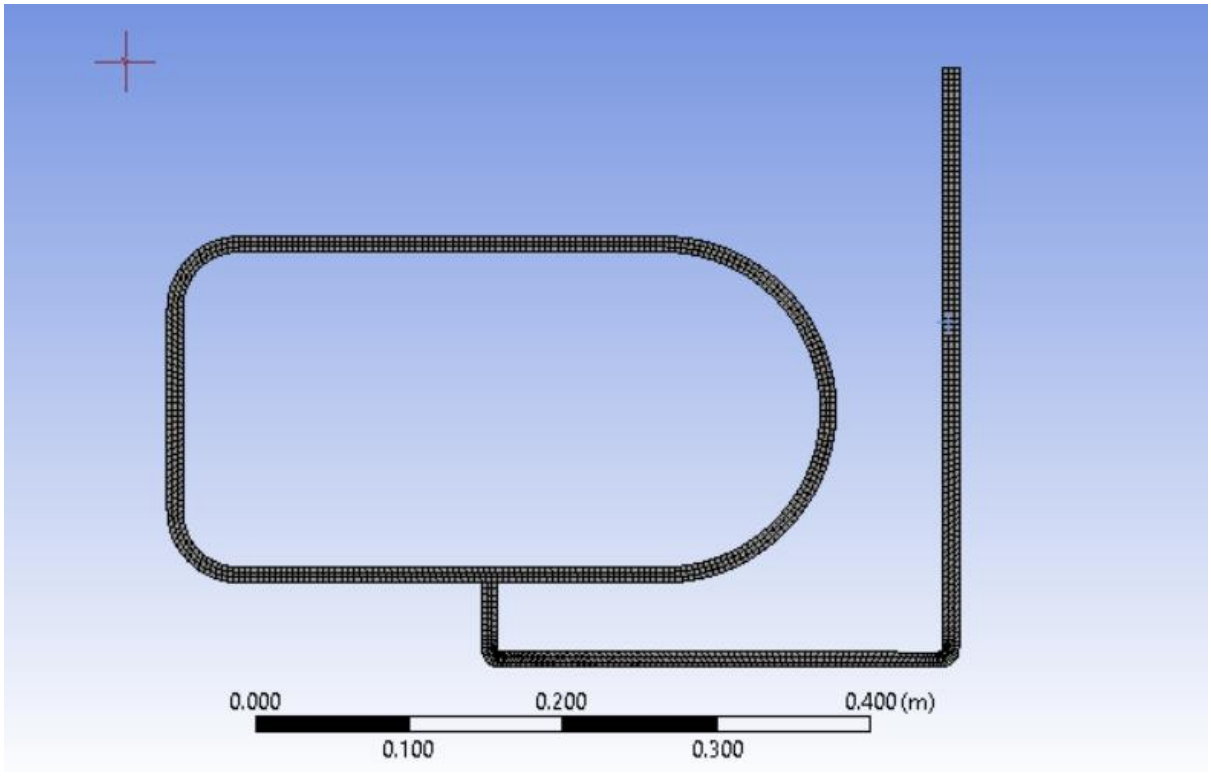

Figure 42. Element size 0.004

Table 9. Sizing details for element of size 0.003 (Case 3)

Element size:	0.003
Element Type:	Quadrilaterals
Number of Nodes:	2576
Number of Element:	1932
Time step size	0.01
Mesh Quality:	Fine
Computational Cost:	Low compared to case 1
Results:	Approximately Same as Physics of Problem and Case 1.

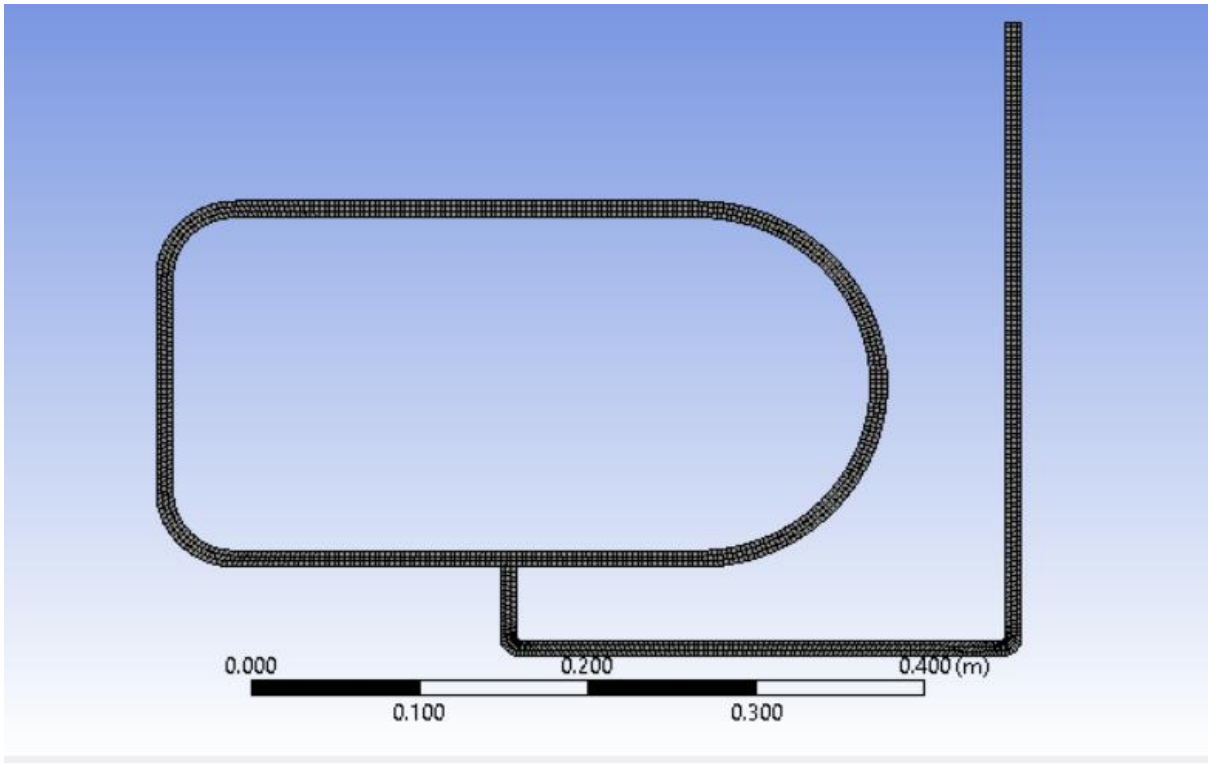

Figure 43. Element size is 0.003

Based on Mesh Independence results element size of 0.003 was selected.

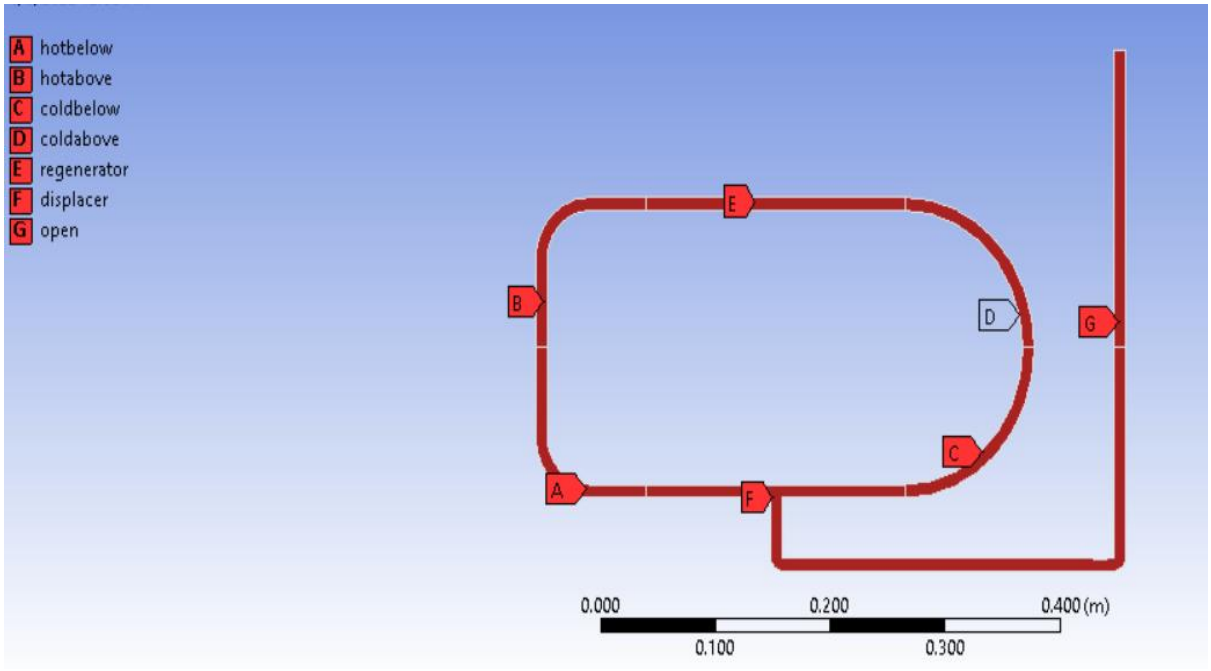

Figure 44. Different Regions for Processing (Specified names of region)

For applying boundary conditions walls have been named, all names have been defined with wall at end because Ansys by name capture type of boundary weather it is inlet, outlet, symmetry or any other.

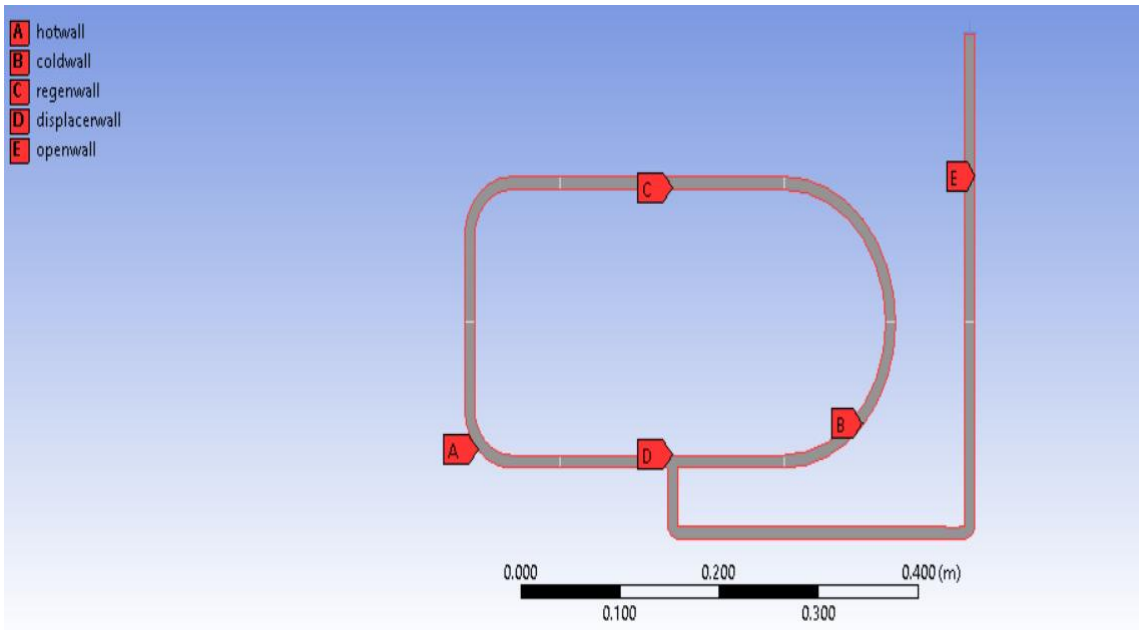

Figure 45. Walls for Boundary Condition

5.2.3.3 Setup

Heating and cooling of air and water changing to vapor and going back is a transient phenomenon. Effects of gravity is considered with other details given below.

Table 10. General setting options for transient formulation

Solver	Pressure-Based
Velocity Formulation	Absolute
Time	Transient
2D Space	Planar
Gravity	-9.81(Y-Axis)

LPSE involve 3 fluids

- Liquid
- Vapor
- Air

Solid

- Copper

Multiphase

In ANSYS FLUENT, there are three different multiphase models using Euler-Euler approach: the volume of fluid model, the mixture model and the Eulerian model. In the VOF model, it is assumed that two or more phases are not interpenetrating, and the volume fractions of all phases sum to unity in every control volume. The VOF model is designed for two or more immiscible fluids where the position of the interface between the fluids is of interest, such as stratified flows, free-surface flows, the motion of large bubbles in a liquid, and the steady or transient tracking of any liquid-gas interface. Therefore, the volume of fluid (VOF) method in ANSYS FLUENT has been applied to simulate liquid Piston Stirling Engine. Number of Eulerian phases are set to be 3.

Implicit body force is selected so this will be unconditionally stable in case of unchecking, CFL number must be specified which should be less than 1 for explicit scheme.

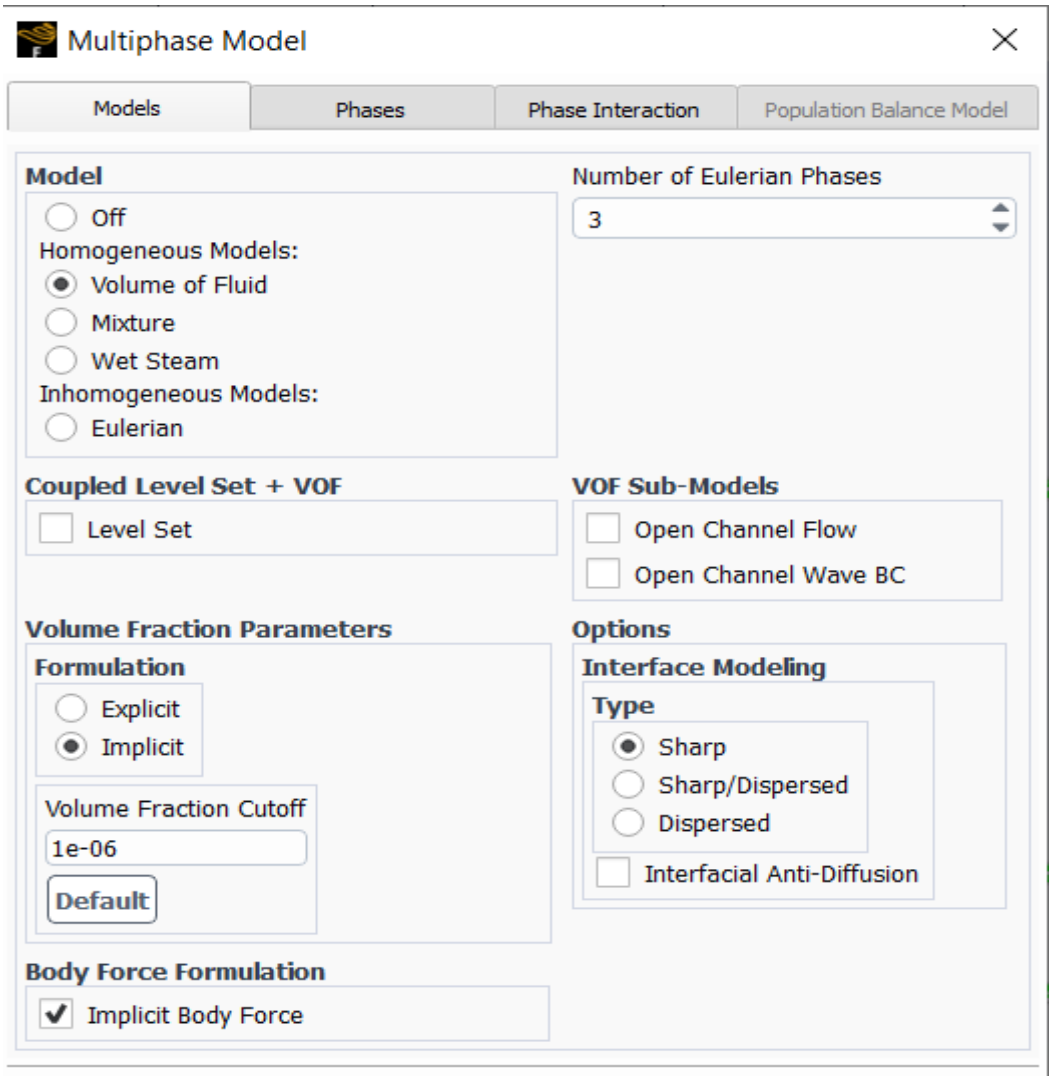

Figure 46. Multiphase Model

Table 11. Fluids during the operation of Engine

Primary Phase	Air
Secondary Phase	Water
Secondary Phase	Vapor

To include the effects of surface tension the continuum surface force (CSF) model was implemented.

Table 12. Surface tension between different Phases.

Phase	Surface Tension(N/m)
Air-Water	0.072
Water-Vapor	0.072
Vapor-Air	0.072

For evaporation and condensation of water mass transfer was included. Lee evaporation condensation was implemented with saturation temperature of 373K.

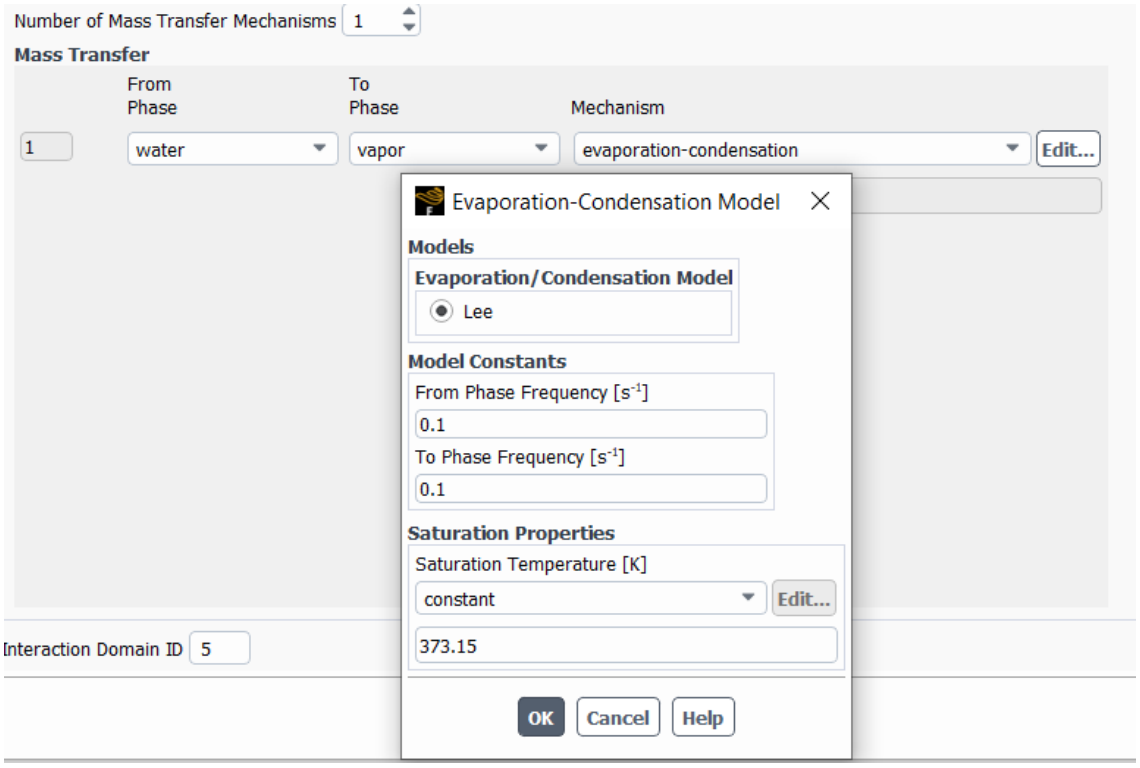

Figure 47. Evaporation Condensation Model considering mass transfer

Turbulence Model, K-Epsilon model with enhanced wall treatment.

5.2.3.4 Boundary Conditions

Heat flux input is applied at hot below wall and convective at hot above wall while cold end was maintained at constant temperature while other walls remain adiabatic.

Table 13. Different types of Boundary Conditions applied at wall

Wall	Boundary Condition	Thermal	Momentum
Hot above Wall	Constant Temperature	380K	No Slip, Stationary wall
Cold Wall	Constant Temperature	308K	No Slip, Stationary wall
Regenerator Wall	Adiabatic	Q = 0	No Slip, Stationary wall
Displacer Wall	Adiabatic	Q = 0	No Slip, Stationary wall
Open wall	Adiabatic	Q = 0	No Slip, Stationary wall

While testing physical model atmospheric pressure measured with pressure sensor was 93kPa. Hence in operating conditions pressure was set to 93kPa with other conditions.

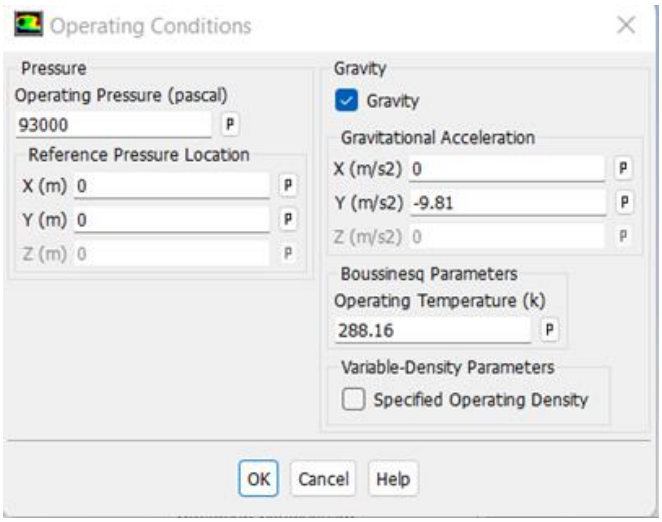

Figure 48. Operating Conditions

Residual which is difference between previous iteration set to be 0.0001.

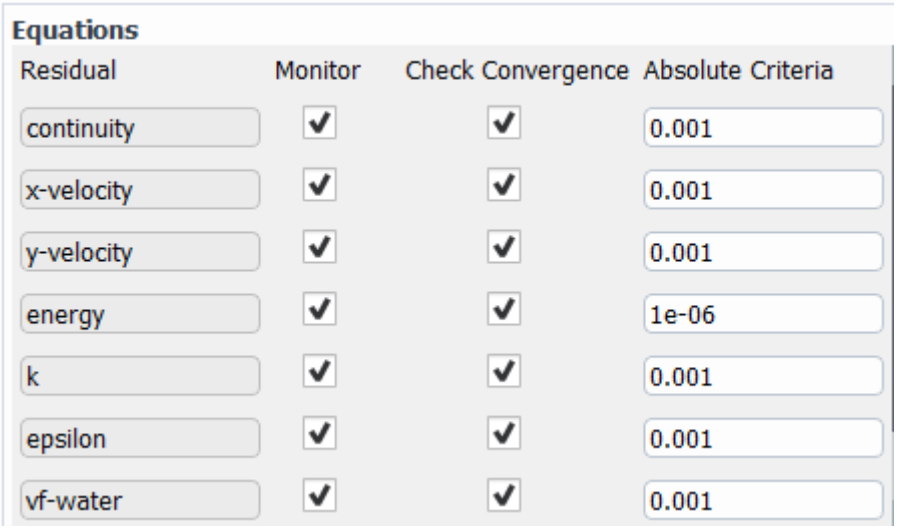

Figure 49. Residual Monitors

5.2.3.5 Solution

Pressure based solver is employed. Pressure appears in all three momentum equations and velocity appear in continuity equation. To couple both we use Pressure-Velocity Coupling. Numerical method used for solving Navier Stokes Equation (NS) is SIMPLE. SIMPLE algorithm is a widely used numerical procedure to solve the Navier–Stokes equations. SIMPLE is an acronym for Semi-Implicit Method for Pressure Linked Equations. Following Settings have been employed for SIMPLE Algorithm. Volume fraction set to Modified HRIC and transient formulation is Second order implicit to have better accuracy in time.

Problem is initialized with gauge pressure set to 0 Pa and temperature set to 308K. Air, water and vapor were patched in respective zone with 0 volume fraction of vapor and volume fraction of 1 for hot below, cold below and displacer region during initialization.

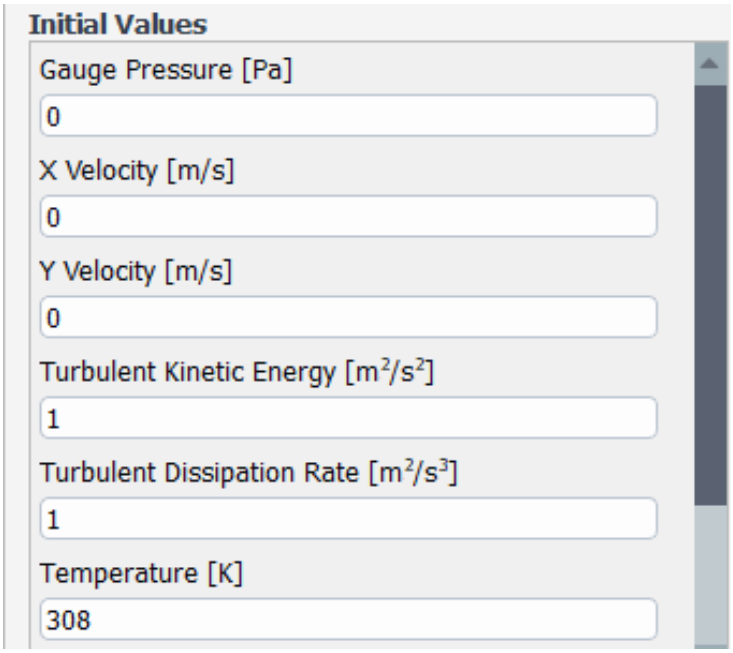

Figure 50. Initialization parameters

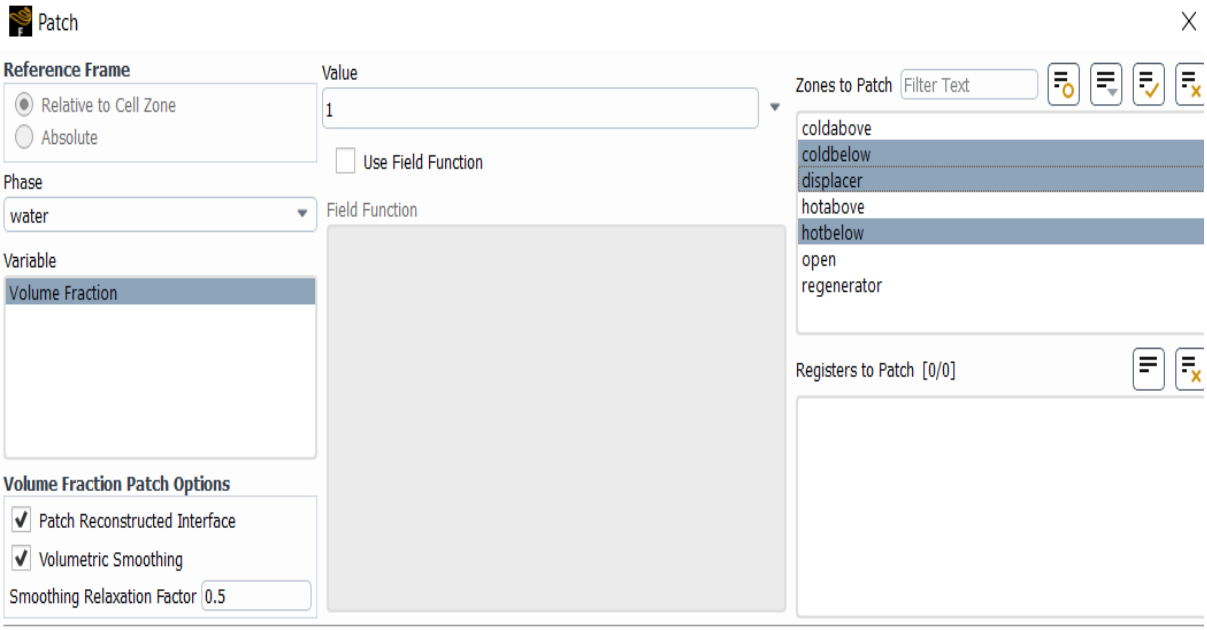

Figure 51. Patching of water initially present in cold below, hot below and displacer

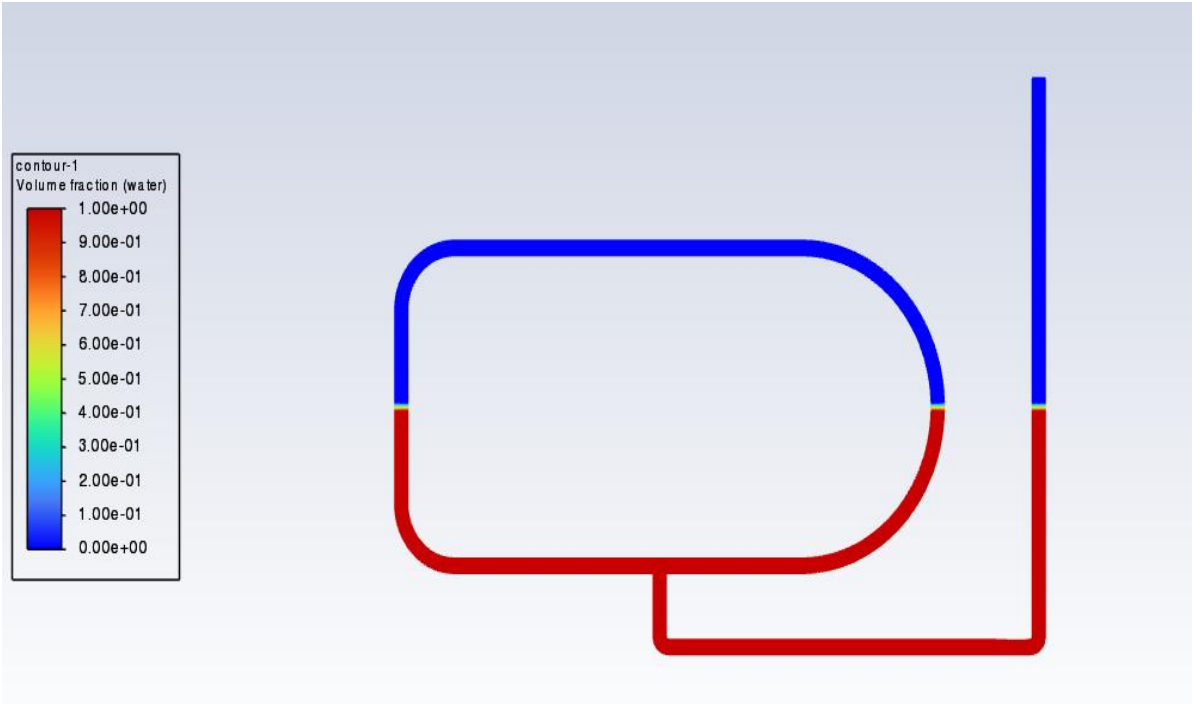

Figure 52. Volume fraction of water

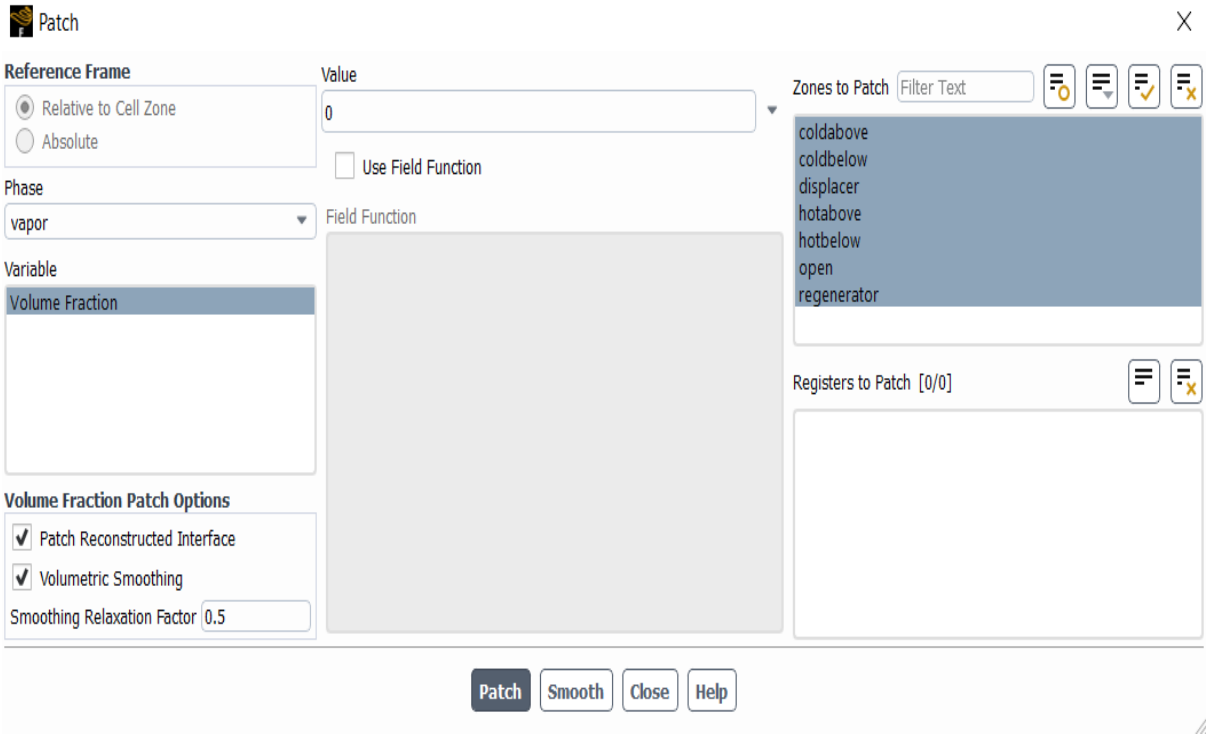

Figure 53. Patching of vapors which are initially zero.

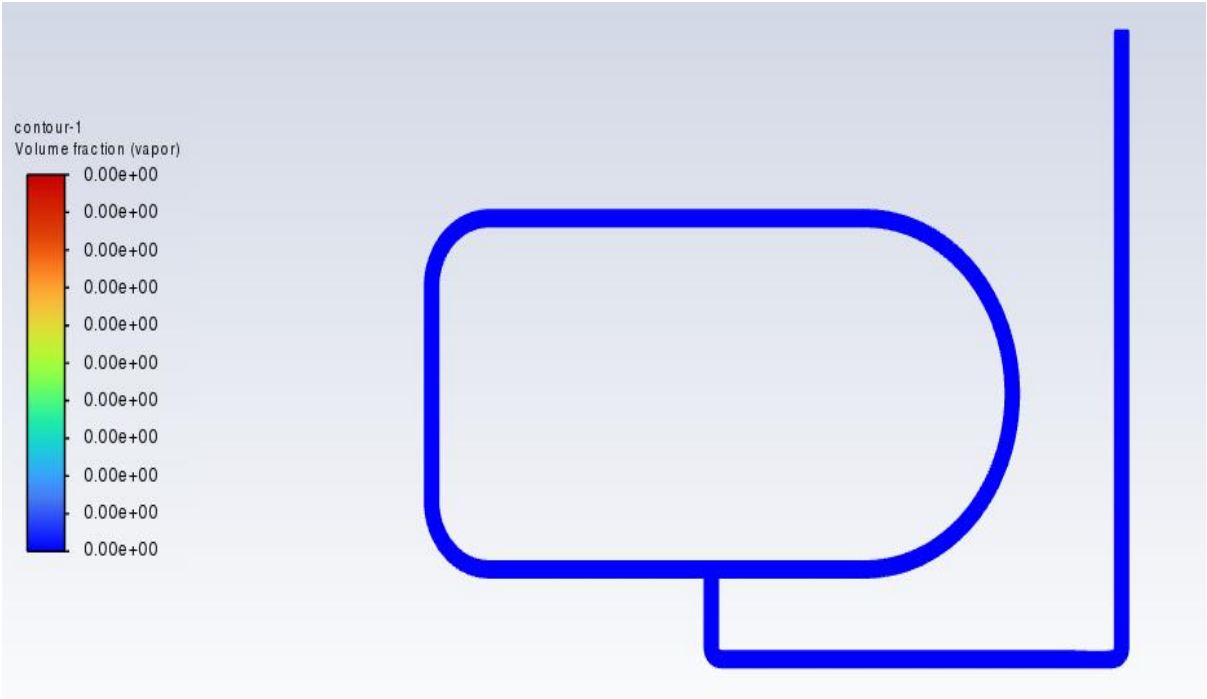

Figure 54. Volume fraction of vapor at t=0

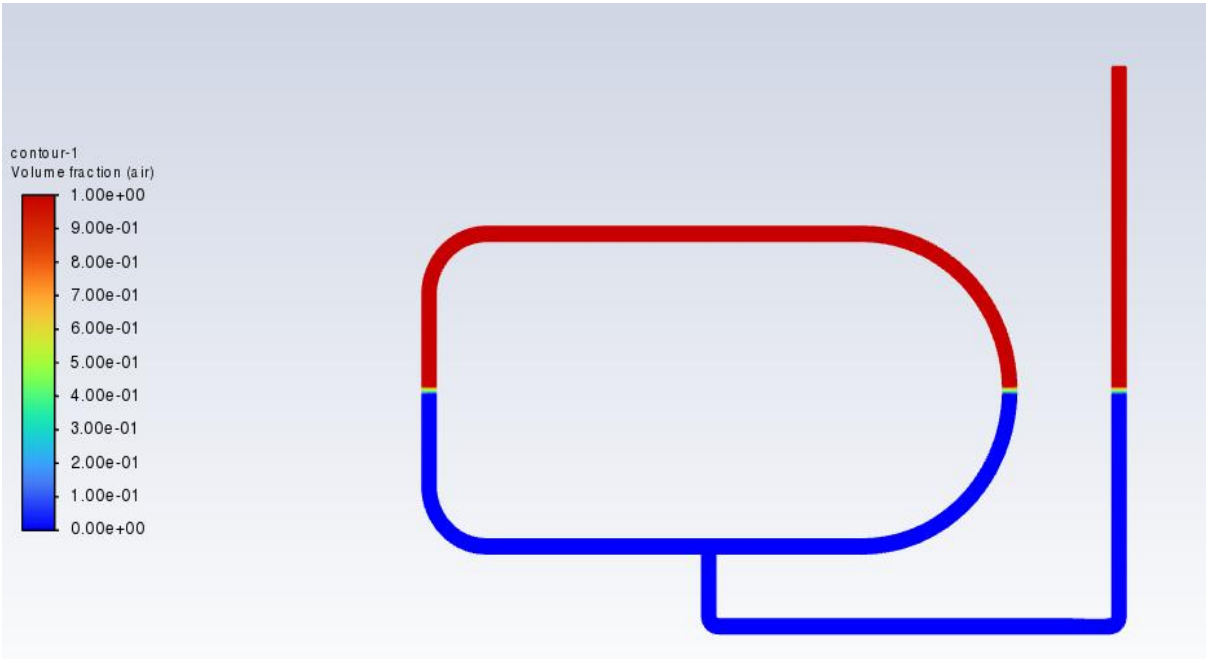

Figure 55. Volume fraction (air)

Table 14. Run calculation parameters

Time Stepping Method	Fixed
Time Step Size	0.01
Number of Time Step	30000

5.3.2.6 Results

Values are calculated at time when oscillations are about to start vapours started to develop.

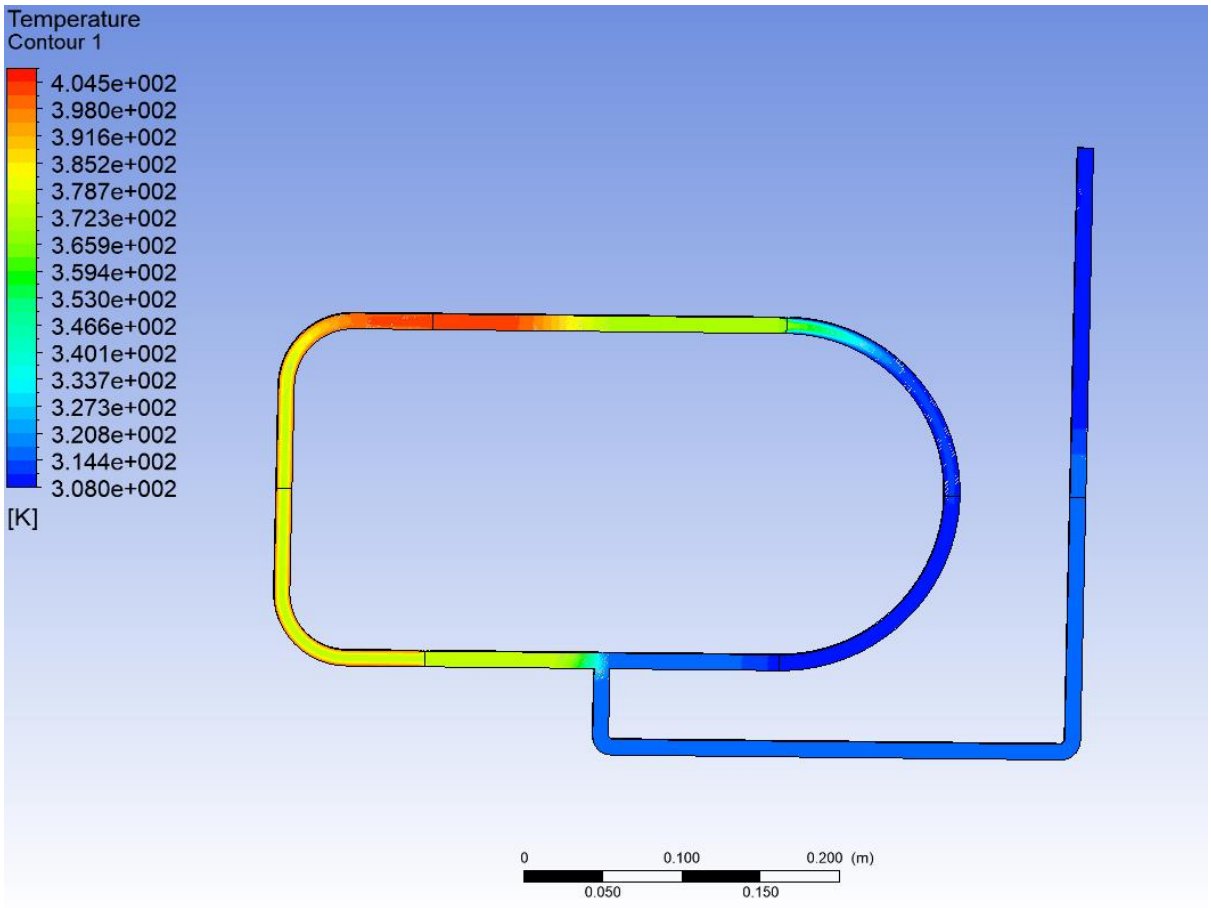

Figure 56. Temperature contour

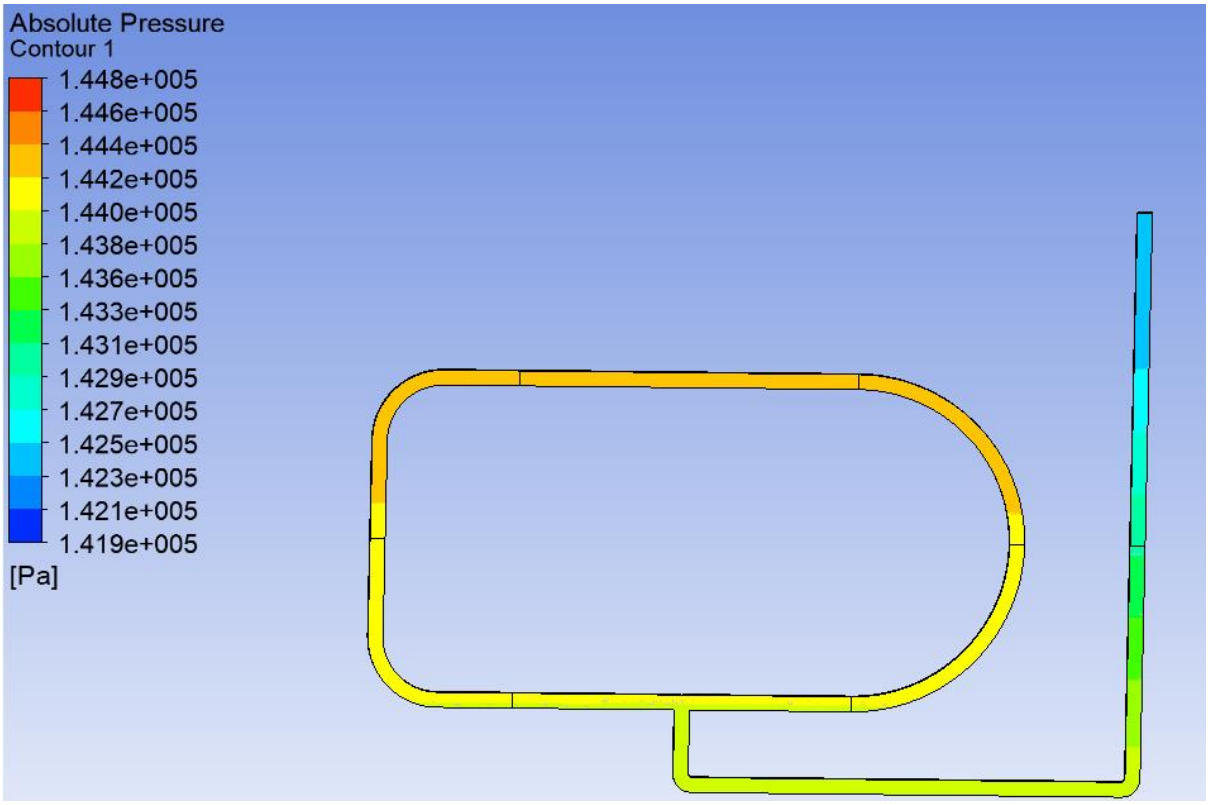

Figure 57. Pressure contour

5.3.2.7 Validation

For validation temperature and pressure results are compared with actual model. Water level in both cases is same which is kept 100ml. Due to assumptions involved in modelling. Difference between the experimental and numerical values occurred.

In actual model oscillation starts after 70 to 80s however during the simulation oscillation start at about 2 minutes. Also, amplitude of oscillation is very small observed during the simulation compared to actual magnitude of oscillation.

Pressure values at cold end from actual experiment differ from simulation values. Graphs showing values in both cases have been shown.

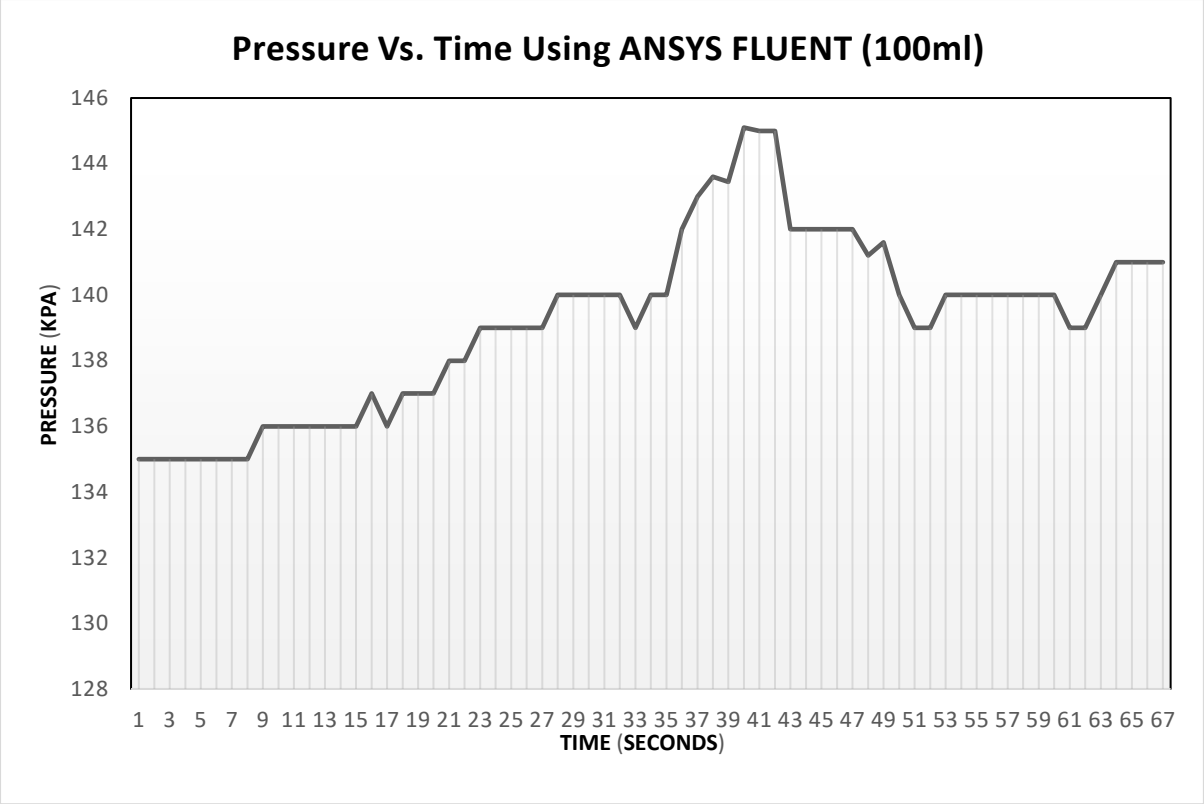

Figure 58. Pressure vs time using Ansys Fluent for 100 ml

Error between both results is about 30-35%.

Temperature values at cold end from actual experiment differ from simulation values. Graphs showing values in both cases have been shown.

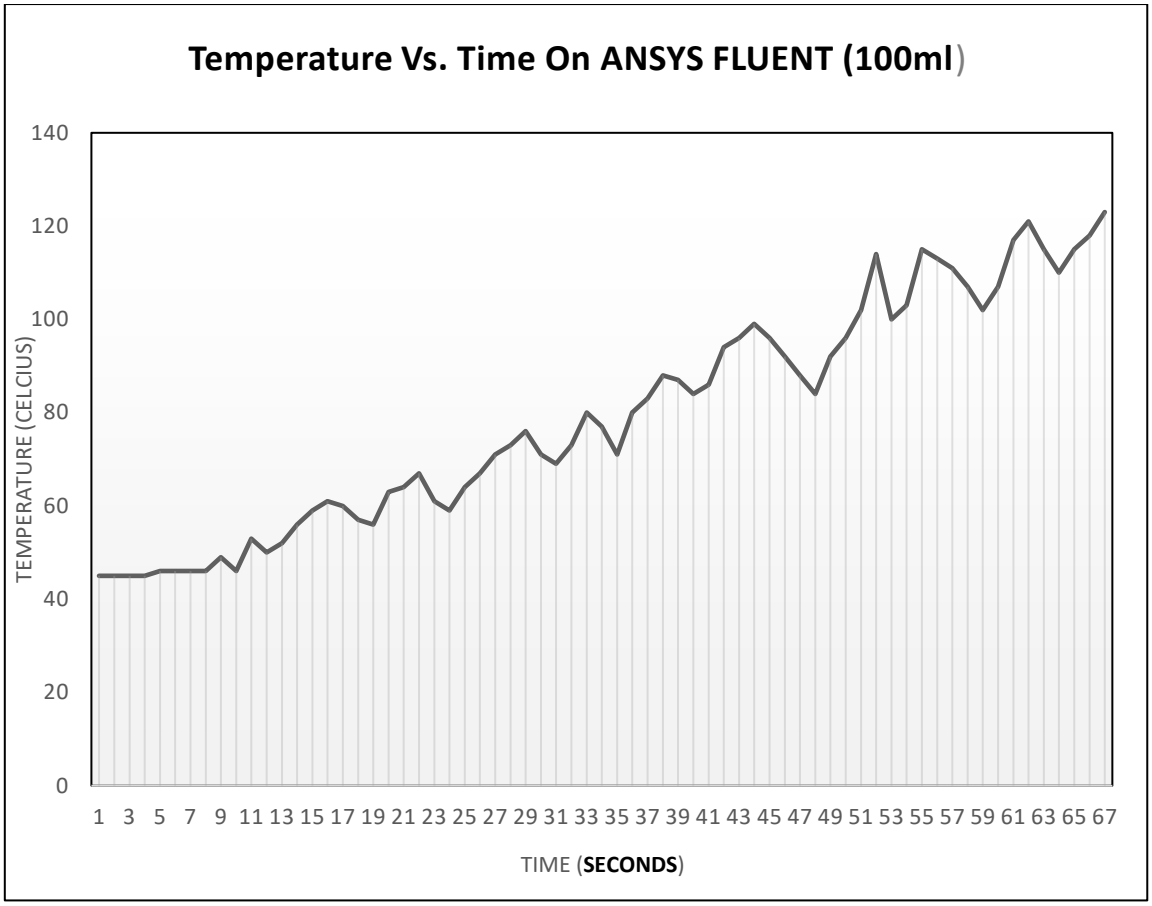

Figure 59. Temperature vs time using Ansys Fluent for 100 ml

Error between both results is about 25-30%.

6 Conclusion

Trends established in our research for the development of a liquid piston Stirling engine included that an engine works at higher capacities of pumping water when the working liquid volume is in bulk in the displacer, hot column and cold column, use of liquid compositions resulting in lower heat of vaporization show higher potentials of energy harvesting for fluidyne engines. The trend in the readings obtained for temperature and pressure is also validated through a CFD model of the fluidyne engine in our research

6.1 Shortcomings

Many setbacks were faced in this whole process. These include the failure of non-returning valve. The non-returning valve present in the market were of high-pressure operation not applicable for our use. Hence, these valves were to be made by us which presented problems of leakages, frictional losses, and unreliability. These valves came in their final useable shape after countless ramifications which was a very hectic procedure. Other than this, challenges faced included pipe leakages, material availability and over-heating.

Similarly, list of challenges was faced in the testing and experimentation phase of the project where the unreliability of the engine, overheating of the system, over pressurizing of the system and unforeseen leakages of the system which made testing a very lengthy process and difficult to attain reliable data. The configuration of sensors was another issue in this phase, due to budget constraints there was only one connector present at a time, this led to separate testing for temperature and pressure readings in the cold column.

CFD Analysis was performed using Ansys fluent with Multiphase Volume of fluid (VOF) approach used for modelling. The assumptions were taken regarding the wall temperature and conditions. Crucial part in this analysis was to have small step size otherwise this phenomenon could not be captured. Values of pressure, temperature and amplitude of oscillation were

compared with empirical data. Amplitude of oscillations in case of ANSYS simulation are very small compared to experimental simulation. Error between pressure and temperature values was around 25% to 30%.

6.2 Future Recommendations

The liquid piston engine demonstrates a unique operation not thoroughly understood in modern engineering. By further understanding and optimizing this cycle which operates on a two-phase oscillation of a working liquid: more powerful and efficient mechanisms can be created. By further exploring this field the simple, low maintenance, and easily manufactured engines could become an important part of how we manage water and waste energy. The operating temperatures for Fluidyne engines in usual practice are less than a 100°C. Hence, in a developing country like Pakistan with a high solar potential there is immense potential to utilize this low-grade thermal energy. In its vast irrigation sector sustainable water pumping can be realized with their use and provide recovery of low-grade wastes even from the industrial sector.

The CFD simulations carried out in this research can be performed more accurately by increasing time step size, also in actual experiment heat input is applied and temperature of hot end varies as function of time. For putting temperature as function of time User Defined Function (UDF) needs to be defined, also there might be some problem in defining physics of problem. Very fine mesh is required to capture evaporation condensation phenomenon hence, mesh quality can be improved. By applying above mentioned recommendations simulations results could be made more closer to the actual experimental results and actual physics of problem would be captured.

Research in this unexplored field is important to be motivated and encouraged to reach higher potentials of this system. Fluidyne engine and their models also attract start-up models for

young entrepreneurs. An example of this is the three-member student team that formed a company with the Georgia Tech's start up summer program to explore the viability of these engines, and their corresponding manuals, as products used in schools. The goal of this start up is to create a concise and accessible laboratory experience for high school and undergraduate students.

References

[1] Y. A. C. &. M. A. Boles, THERMODYNAMICS An Engineering Approach, McGraw-Hill Education, 2005.

[2] S. Newlan, "ANALYSIS, OPTIMIZATION, AND APPLICATION OF THE LIQUID PISTON HEAT ENGINE THROUGH DESIGN AND EMPIRICAL MODELLING", Georgia Institute of Technology, 2017.

[3] A. Gupta, S. Sharma, and S. Narayan, Liquid Piston Engines (John Wiley and Sons, Hoboken, 2017).

[4] Wang K, Sanders SR, Dubey S, Choo FH, Duan F. Stirling cycle engines for recovering low and moderate temperature heat: a review. Renew Sustain Energy Rev. 2016; 62:89-108. https://doi.org/10.1016/j.rser.2016.04.031

[5] West CD. The Fluidyne heat engine. AERE R6775, UKAEA Atomic Energy Research Establishment, Harwell, UK; 1971.

[6] Goldberg LF, Rallis CJ, Bell AJ, Urieli I. Some experimental results on laboratory model Fluidyne engines. In: Proceedings of 12th intersociety energy conversion engineering conference, Washington, D.C., USA; 1977.

[7] Bell AJ, Goldberg LF. The Fluidyne engine. Final-year laboratory project, University of

the Witwatersrand; 1976.

[8] Stammers CW. The operation of the Fluidyne heat engine at low differential temperatures.

J Sound Vib 1979;63(4):507–16

[9] Ning Yang, Robert Rickard, Kevin Pluckter, and Todd Sulcheka) George W. Woodruff School of Mechanical Engineering and Parker H. Petit Institute for Bioengineering and Bioscience, Georgia Institute of Technology, Atlanta, Georgia 30332, USA

[10] Orda E, Mahkamov J. Development of 'low-tech' solar thermal water pumps for use in developing countries. J Sol Energy Eng 2004; 126:768–73

[11] Characterization of a solar-powered fluidyne test bed Jackson W. Mason, James W. Stevens University of Colorado at Colorado Springs, Colorado Springs, CO, USA.

[12] Mason JW, Stevens JW. Design and construction of a solar-powered Fluidyne test bed. In: Proceedings of ASME 2011 international mechanical engineering congress and exposition, Denver, Colorado, USA; 2011. p. 9-20.

[13] Bell GC. Solar powered liquid piston Stirling cycle irrigation pump. NASA STI/ Recon Technical Report N, USA; 1979.

[14] Mosby DC. The Fluidyne heat engine [Master thesis] Monterey, CA, USA: Naval Postgraduate School; 1978.

[15] F. KYEI- MANU, “Design & Development of a Liquid Piston Stirling Engine”, E90 Senior Design Project Report, 2006.

[16] O. A. Oyewunmi, C. J. W. Kirmse, A. J. Haslam, E. A. Müller, and C. N. Markides, “Working-fluid selection and performance investigation of a two-phase single-reciprocating-piston heat-conversion engine,” Appl. Energy, vol. 186, pp. 376–395, 2017.